Geosci. Model Dev. Discuss., 8, 8009–8062, 2015
www.geosci-model-dev-discuss.net/8/8009/2015/
doi:10.5194/gmdd-8-8009-2015


Geoscientific Model Development Discussions
Open Access





# FPLUME-1.0: An integrated volcanic plume model accounting for ash aggregation

*A one-dimensional, integral*

**A. Folch[1], A. Costa[2], and G. Macedonio[3]**

[1]CASE Department, Barcelona Supercomputing Center, Barcelona, Spain
[2]Istituto Nazionale di Geofisica e Vulcanologia, Sezione di Bologna, Italy
[3]Istituto Nazionale di Geofisica e Vulcanologia, Sezione di Napoli, Italy

Received: 22 July 2015 – Accepted: 24 August 2015 – Published: 17 September 2015

Correspondence to: A. Folch (arnau.folch@bsc.es)

Published by Copernicus Publications on behalf of the European Geosciences Union.





## Abstract

*"bent over" should be used throughout the paper as an adjective, not as a noun*

Eruption Source Parameters (ESP) characterizing volcanic eruption plumes are crucial inputs for atmospheric tephra dispersal models, used for hazard assessment and risk mitigation. We present FPLUME-1.0, a steady-state 1-D cross-section averaged eruption column model based on the Buoyant Plume Theory (BPT). The model accounts for plume bent over by wind, entrainment of ambient moisture, effects of water phase changes, particle fallout and re-entrainment, a new parameterization for the air entrainment coefficients and a model for wet aggregation of ash particles in presence of liquid water or ice. In the occurrence of wet aggregation, the model predicts an "effective" grain size distribution depleted in fines with respect to that erupted at the vent. Given a wind profile, the model can be used to determine the column height from the eruption mass flow rate or vice-versa. The ultimate goal is to improve ash cloud dispersal forecasts by better constraining the ESP (column height, eruption rate and vertical distribution of mass) and the "effective" particle grain size distribution resulting from eventual wet aggregation within the plume. As test cases we apply the model to the eruptive phase-B of the 4 April 1982 El Chichón volcano eruption (México) and the 6 May 2010 Eyjafjallajökull eruption phase (Iceland).

## 1 Introduction

Volcanic plumes (e.g. Sparks, 1997) are ~~a~~ multiphase flows containing volcanic gas, entrained ambient air and moisture and suspended tephra, consisting on both juvenile (resulting from magma fragmentation), crystal and lithic (resulting from wall rock erosion) particles ranging from meter-sized blocks to micron-sized fine ash (diameter ≤ 63 µm). Sustained volcanic plumes present a basal jet thrust region where the mixture rises due to its momentum. As ambient air is entrained by turbulent mixing, it heats and expands, thereby reducing the *average* density of the mixture. ~~It~~ leads a transition to the convective region, in which positive buoyancy drives the mixture upwards above

*these cannot be mentioned among the "suspended" tephra!*

*Air entrainment*

the so-called Neutral Buoyancy Level (NBL), where the mixture density equals that of the surrounding atmosphere. For strong plumes, excess of momentum above the NBL (overshooting) can effectively drive the mixture higher forming the umbrella region, where tephra disperses horizontally first as a gravity current (e.g. Costa et al., 2013) and then under passive wind advection forming a volcanic cloud (see Fig. 1). Depending on the balance between the ascending plume velocity and the height-dependent horizontal wind velocity, plumes can rise sub-vertically (strong plumes) or bent-over spreading laterally around the NBL, often without developing an umbrella region (weak plumes).

Characterization ~~trough~~ through observations and monitoring and modeling of volcanic plumes is essential to provide realistic source terms to atmospheric dispersal models, aimed at simulating atmospheric tephra transport and/or the resulting fallout deposit (e.g. Folch, 2012). Plume models range in complexity from 1-D ~~integrated~~ integral models ~~build~~ built upon the Buoyant Plume Theory (BPT) of Morton et al. (1956) to sophisticated multiphase Computational Fluid Dynamics (CFD) models (e.g. Suzuki et al., 2005; Esposti Ongaro et al., 2007; Suzuki and Koyaguchi, 2009, 2013; Herzog and Graf, 2010). The latter group of models are valuable to understand physical phenomena and the role of different parameters but, given ~~its~~ their high computational cost, coupling with atmospheric dispersal models at an operational level is still unpractical. For this reason, simpler 1-D cross-section averaged models or even empirical relationships between plume height and eruption rate (e.g. Mastin et al., 2009; Degruyter and Bonadonna, 2012) are used in practice to furnish Eruption Source Parameters (ESP) to atmospheric transport models, the results of which strongly depend on the source term quantification (i.e. determination of plume height, eruption rate, vertical distribution of mass and particle grain size distribution).

Many plume models based on the BPT have been proposed after the seminal studies of Wilson (1976) and Sparks (1986) to address different aspects of plume dynamics. For example, Woods (1988, 1993) proposed a model to include the latent heat associated with condensation of water vapor and quantify its effects upon the eruption col-





umn. Ernst et al. (1996) presented a model considering particle sedimentation and re-entrainment from plume margins. Bursik (2001) analyzed how the interaction with wind enhances entrainment of air, plume bending, and decrease of the total plume height for a given eruption rate. Several other plume models exist (e.g. Mastin, 2007; Degruyter and Bonadonna, 2012; Woodhouse et al., 2013; Devenish, 2013; de' Michieli Vitturi et al., 2015) considering different modelling approaches, simplifying assumptions and model parameterizations. It is well recognized that the values of the air entrainment coefficients have a large influence on the results of the plume models. On the other hand, volcanic ash aggregation (e.g. Brown et al., 2012) can occur within the eruption column or, under certain circumstances, downstream within the ash cloud (Durant et al., 2009). In any case, the formation of ash aggregates (with typical sizes around few hundreds of µm and less ~~denser~~ dense than the primary particles) dramatically impacts particle transport dynamics thereby reducing the atmospheric residence time of aggregating particles and promoting the premature fallout of fine ash. As a result, atmospheric transport models neglecting aggregation tend to overestimate far-range ash cloud concentrations, leading to an overestimation of the risk posed by ash clouds on civil aviation and an underestimation of ash loading in the near field. So far, no plume model tries to predict the formation of ash aggregates in the eruptive column and how it affects the particle grain size distribution erupted at the vent. This can be explained in part because aggregation mechanisms are complex and not fully understood yet, although theoretical models have been proposed for wet aggregation (Costa et al., 2010; Folch et al., 2010).

Here we present FPLUME-1.0, a steady-state 1-D cross-section averaged plume model which accounts for plume bent over, entrainment of ambient moisture, effects of water phase changes on the energy budget, particle fallout and re-entrainment by turbulent eddies, variable entrainment coefficients fitted from experiments, and particle aggregation in presence of liquid water or ice that depends on plume dynamics, particle properties, and amount of liquid water and ice existing in the plume. The modeling of aggregation in the plume, proposed here for the first time, allows our model to predict an “effective” Total Grain Size Distribution (TGSD) depleted in fines with respect to that erupted at the vent. The ultimate goal is to improve ash cloud forecasts by better constraining this relevant ~~aspect~~ of the source term. In this manuscript, we present first the governing equations for the plume and aggregation models and then apply the combined model to two test cases, the eruptive phase-B of the 1982 El Chichón volcano eruption (México) and the 6 May 2010 Eyjafjallajökull eruption phase (Iceland).

*aspects*

## 2 Physical plume model

We consider a volcanic plume as a multiphase mixture of volatiles, suspended particles (tephra) and entrained ambient air. For simplicity, water (in vapor, liquid or ice phase) is assumed the only volatile specie, being either of magmatic origin or incorporated trough the ingestion of moist ambient air. Erupted tephra particles can form by magma fragmentation or by erosion of the volcanic conduit, and can vary notably in size, shape and density. For historical reasons, field volcanologists describe the continuous spectrum of particle sizes in terms of the dimensionless Φ-scale (Krumbein, 1934):

$$d(\Phi) = d_* 2^{-\Phi} = d_* e^{-\Phi \log 2} \tag{1}$$

where $d$ is the particle size and $d_* = 10^{-3}$ m is a reference length (i.e. $2^{-\Phi}$ is the direction-averaged particle size expressed in mm). The vast majority of modeling strategies, discretize the continuous particle Grain Size Distribution (GSD) by grouping particles in $n$ different Φ-bins, each with an associated particle mass fraction (the models based on moments e.g. de' Michieli Vitturi et al., 2015 are the exception). Because particle size exerts a primary control on sedimentation, Φ-classes are often identified with terminal settling velocity classes although, strictly, a particle settling velocity class is univocally defined not only by particle size but also by its density and shape. We propose a model for volcanic plumes as a multiphase homogeneous mixture of water (in any phase), entrained air, and $n$ particle classes, including a parameterization for the air entrainment coefficients and a wet aggregation model. Because the governing





equations based upon the BPT are not adequate above NBL, we also propose a new semi-empirical model to describe such a region.

### 2.1 Governing equations

The steady-state cross-section averaged governing equations for axisymmetric plume motion in a turbulent wind are (see Fig. 1):

$$\frac{d\hat{M}}{ds} = 2\pi r \rho_a u_e + \sum_{i=1}^{n} \frac{d\hat{M}_i}{ds} \tag{2a}$$

$$\frac{d\hat{P}}{ds} = \pi r^2 (\rho_a - \hat{\rho}) g \sin\theta + u_a \cos\theta (2\pi r \rho_a u_e) + \hat{u} \sum_{i=1}^{n} \frac{d\hat{M}_i}{ds} \tag{2b}$$

$$\hat{P}\frac{d\theta}{ds} = \pi r^2 (\rho_a - \hat{\rho}) g \cos\theta - u_a \sin\theta (2\pi r \rho_a u_e) \tag{2c}$$

*A mass loss term is missing (see text)*

$$\frac{d\hat{E}}{ds} = 2\pi r \rho_a u_e \left( c_a T_a + gz + \frac{1}{2}u_e^2 \right) + c_p \hat{T} \sum_{i=1}^{n} \frac{d\hat{M}_i}{ds} + L_c \frac{d}{ds}\left(\hat{M}\hat{x}_l\right) + L_d \frac{d}{ds}\left(\hat{M}\hat{x}_s\right) \tag{2d}$$

$$\frac{d\hat{M}_a}{ds} = 2\pi r \rho_a u_e (1 - w_a) \tag{2e}$$

$$\frac{d\hat{M}_w}{ds} = 2\pi r \rho_a u_e w_a \tag{2f}$$

$$\frac{d\hat{M}_i}{ds} = \frac{\chi}{r\hat{u}} \left( \frac{f u_e}{dr/ds} - u_{si} \right) \hat{M}_i + A_i^+ - A_i^- \tag{2g}$$

$$\frac{dx}{ds} = \cos\theta \cos\Phi_a \tag{2h}$$

$$\frac{dy}{ds} = \cos\theta \sin\Phi_a \tag{2i}$$

$$\frac{dz}{ds} = \sin\theta \tag{2j}$$

where $\hat{M} = \pi r^2 \hat{\rho}\hat{u}$ is the total mass flow rate, $\hat{P} = \hat{M}\hat{u}$ is the total axial (stream-wise) momentum flow rate, $\theta$ is the plume bent over angle with respect to the horizontal (i.e. $\theta = 90^\circ$ for a plume raising vertically), $\hat{E} = \hat{M}(\hat{c}\hat{T} + gz + \frac{1}{2}\hat{u}^2)$ is the total energy flow rate, $\hat{M}_a$ is the mass flow rate of dry air, $\hat{M}_w = \hat{M}\hat{x}_w$ is the mass flow rate of volatiles (including water vapor, liquid and ice), $\hat{M}_i = \hat{M}\hat{x}_p f_i$ is the mass flow rate of particles of class $i$ ($i = 1:n$), $x$ and $y$ are the horizontal coordinates, $z$ is height, and $s$ is the distance along the plume axis (see Tables 1 and 2 for the definition of all symbols and variables appearing in the manuscript).

The equations above derive from conservation principles assuming axial (stream-wise) symmetry and considering bulk quantities integrated over a plume cross-section using a top-hat profile in which a generic quantity $\phi$ has a constant value $\hat{\phi}(s)$ at a given plume cross-section and vanishes outside (here we refer to section-averaged quantities as "bulk" quantities, denoted by a hat). We have derived these equations by combining formulations from different previous plume models (Netterville, 1990; Woods, 1993; Ernst et al., 1996; Bursik, 2001; Costa et al., 2006; Woodhouse et al., 2013) in order to include in a single model effects from plume bent over by wind, particle fallout and re-entrainment at plume margins, transport of volatiles (water) accounting also for ingestion of ambient moisture, phase changes (water vapor condensation and deposition) and particle aggregation. *Headline* Equation (2a) expresses the conservation of total mass, accounting in the Right Hand Side (RHS) for the mass of air entrained through the plume margins and the loss/gain of mass by particle fallout/re-entrainment. Equations (2b) and (2c) express the conservation of axial (stream-wise) and radial momentum respectively, accounting in the RHS for contributions from buoyancy (first term), entrainment of air, and particle fallout/re-entrainment. Note that the buoyancy term, acting only along the vertical direction $z$, acts as a sink of momentum in the basal gas-thrust jet region (where $\hat{\rho} > \rho_a$) and as a source of momentum where the plume is positively buoyant ($\hat{\rho} < \rho_a$). Equation (2d) express the conservation of energy, accounting in the RHS for



gain of energy (enthalpy, potential and kinetic) by ambient air entrainment (first term), loss/gain by particle fallout/re-entrainment (second term), and gain of energy by conversion of water vapor into liquid (condensation) or into ice (deposition). Equations (2e), (2f) and (2g) express, respectively, the conservation of mass of dry air, water (vapor, liquid and ice) and solid particles. The latter set of equations, one for each particle class, account in the RHS for particle re-entrainment (first term), particle fallout (second term) and particle aggregation. Here we have included two terms ($A_i^+$ and $A_i^-$) that account for the creation of mass from smaller particles aggregating into particle class $i$ and for the destruction of mass resulting from particles of class $i$ contributing to the formation of larger-size aggregates. Finally, Eqs. (2h) to (2j) determine the 3-D plume trajectory as a function of the length parameter $s$. All these equations constitute a set of $9+n$ first order ordinary differential equations in $s$ for $9+n$ unknowns: $\hat{M}$, $\hat{P}$, $\theta$, $\hat{E}$, $\hat{M}_a$, $\hat{M}_w$, $\hat{M}_i$ (for each particle class), $x$, $y$ and $z$. Note that, using the definitions of $\hat{M}$-$\hat{P}$-$\hat{E}$, the equations can also be expressed in terms of $\hat{u}$-$r$-$\hat{T}$ given the bulk density.

Assuming an homogeneous mixture, the bulk density $\hat{\rho}$ of the mixture is:

$$\frac{1}{\hat{\rho}} = \frac{\hat{x}_p}{\rho_p} + \frac{\hat{x}_l}{\rho_l} + \frac{\hat{x}_s}{\rho_s} + \frac{(1 - \hat{x}_p - \hat{x}_l - \hat{x}_s)}{\rho_g} \tag{3}$$

where $\hat{x}_p$, $\hat{x}_l$ and $\hat{x}_s$ are, respectively, the mass fractions of particles, liquid water and ice, $\rho_p$ is the class-averaged particle (pyroclasts) density, $\rho_l$ and $\rho_s$ are liquid water and ice densities, and $\rho_g$ is the gas phase (i.e. dry air plus water vapor) density. We assume that $\rho_g \approx \rho_a(\hat{T})$ where $\rho_a$ is the air density (at the bulk temperature). *Not needed! see text* Under the assumption of mechanical equilibrium (i.e. assuming the same bulk velocity $\hat{u}$ for all phases and components) is holds that:

$$\hat{x}_p = \frac{\sum \hat{M}_i}{\hat{M}} = \frac{\sum \hat{M}_i}{\sum \hat{M}_i + \hat{M}_w + \hat{M}_a} \tag{4}$$

Additional hypothesis are necessary in order to determine how the mass fraction of water ($\hat{x}_w = \hat{x}_v + \hat{x}_l + \hat{x}_s$) distributes amongst the different phases depending on temperature and pressure. As in Folch et al. (2010), we consider the existence of a freezing temperature ($T_f$) below which all liquid water and vapor in excess (if any) are converted instantaneously to ice (i.e. the three water phases do not coexist in any section of the plume). In addition, and following Woods (1993) and Woodhouse et al. (2013), we also consider that, if the air–water mixture becomes saturated in water vapor, condensation or deposition occur rapidly and the plume remains just saturated. This assumption implies that the partial pressure of water vapor $P_v$:

$$P_v = \frac{\hat{M}\hat{x}_v}{\hat{M}_a + \hat{M}\hat{x}_v} P \tag{5}$$

equals the saturation pressure of vapor over liquid ($e_l$) or over ice ($e_s$) at the bulk temperature, where $P$ is pressure (approximated to the atmospheric pressure at a given height, $P \approx P_a(z)$) and the saturation pressures over liquid and ice are given (in hPa) by (Murphy and Koop, 2005):

$$e_l = 6.112 \exp\left(17.67 \frac{\hat{T} - 273.16}{\hat{T} - 29.65}\right) \tag{6}$$

$$\log e_s = -9.097\left(\frac{273.16}{\hat{T}} - 1\right) - 3.566 \log\left(\frac{273.16}{\hat{T}}\right) + 0.876\left(1 - \frac{\hat{T}}{273.16}\right) + \log(6.1071) \tag{7}$$

Therefore, if $\hat{T} > T_f$ and $P_v < e_l$ the plume is undersaturated and there is no water vapor condensation (i.e. $\hat{x}_v = \hat{x}_w$ and $\hat{x}_l = \hat{x}_s = 0$). In contrast, if $P_v \geq e_l$, the vapor in excess is immediately converted into liquid and:

$$\hat{x}_v = \frac{e_l}{P - e_l}\frac{\hat{M}_a}{\hat{M}} = \frac{e_l}{P - e_l}\left(\frac{\hat{M}_a}{\sum \hat{M}_i + \hat{M}_w + \hat{M}_a}\right)$$





$$\hat{x}_s = 0$$

$$\hat{x}_l = \hat{x}_w - \hat{x}_v = \frac{\hat{M}_w}{\sum \hat{M}_i + \hat{M}_w + \hat{M}_a} - \hat{x}_v \tag{8}$$

On the other hand, if $\hat{T} \leq T_f$ and $P_v < e_s$ the plume is undersaturated and there is no water vapor deposition. In contrast, if $P_v \geq e_s$, the vapor in excess is immediately converted into ice and:

$$\hat{x}_v = \frac{e_s}{P - e_s}\frac{\hat{M}_a}{\hat{M}} = \frac{e_s}{P - e_s}\left(\frac{\hat{M}_a}{\sum \hat{M}_i + \hat{M}_w + \hat{M}_a}\right)$$

$$\hat{x}_l = 0$$

$$\hat{x}_s = \hat{x}_w - \hat{x}_v = \frac{\hat{M}_w}{\sum \hat{M}_i + \hat{M}_w + \hat{M}_a} - \hat{x}_v \tag{9}$$

The latent heat released by water vapor condensation and deposition can provide an important additional source of energy for small to moderate plumes in moist environments (Woods, 1993) and is given by:

$$L_c = L_{co} + (c_v - c_l)(\hat{T} - T_o) \tag{10}$$

$$L_d = L_{do} + (c_v - c_s)(\hat{T} - T_o) \tag{11}$$

where $L_{co} = 2.50 \times 10^6$ and $L_{do} = 2.83 \times 10^6\,\mathrm{J\,kg^{-1}}$ are the latent heats of condensation and deposition at $T_o = 273\,\mathrm{K}$. Assuming thermal equilibrium between water phases, air and particles, the specific heat capacity of the mixture $\hat{c}$ is given by:

$$\hat{c} = \frac{c_p \sum \hat{M}_i + (c_v\hat{x}_v + c_l\hat{x}_l + c_s\hat{x}_s)\hat{M}_w + c_a\hat{M}_a}{\sum \hat{M}_i + \hat{M}_w + \hat{M}_a} \tag{12}$$

For the particle re-entrainment parameter $f$ we adopt the fit proposed by Ernst et al. (1996) using data for plumes not affected by wind:

$$f = 0.43\left(1 + \left[\frac{0.78 u_s P_o^{1/4}}{F_o^{1/2}}\right]^6\right)^{-1} \qquad (13)$$

where $P_o = r_o^2 \hat{u}_o^2$ and $F_o = r_o^2 \hat{u}_o \hat{c}_o \hat{T}_o$ are the specific momentum and thermal fluxes at the vent ($s = 0$). This expression may overestimate re-entrainment for bent over plumes (Bursik, 2001). Finally, particle terminal settling velocity $u_{si}$ is parameterized as (Costa et al., 2006; Folch et al., 2009):

$$u_{si} = \sqrt{\frac{4g(\rho_{pi} - \hat{\rho})d_i}{3C_d\hat{\rho}}} \qquad (14)$$

where $d_i$ is the class particle diameter and $C_d$ is a drag coefficient that depends on the Reynolds number $Re = d_i u_{si}\hat{\rho}/\hat{\mu}$. Several empirical fits exist for drag coefficients of spherical and non-spherical particles (e.g. Wilson and Huang, 1979; Arastoopour et al., 1982; Ganser, 1993; Dellino et al., 2005). In particular, Ganser (1993) gives a fit valid over a wide range of particle sizes and shapes covering the spectrum of volcanic particles considered in volcanic column models (lapilli and ash):

$$C_d = \frac{24}{ReK_1}\left\{1 + 0.1118[Re(K_1K_2)]^{0.6567}\right\} + \frac{0.4305K_2}{1 + \frac{3305}{ReK_1K_2}} \qquad (15)$$

*How is it inverted? (see text)*

where $K_1$ and $K_2$ are two shape factors depending on particle sphericity, $\Psi$, and particle orientation.

Given a closure equation for the turbulent air entrainment velocity $u_e$, and an aggregation model (defining the mass aggregation coefficients $A_i^+$ and $A_i^-$), Eqs. (2a) to (2i)



can be integrated along the plume axis from the inlet (volcanic vent) up to the neutral buoyancy level. Inflow (boundary) conditions are required at the vent ($s = 0$) for, e.g., total mass flow rate $\hat{M}_o$, bent over angle $\theta_o = 90°$, temperature $\hat{T}_o$, exit velocity $\hat{u}_o$, fraction of water $\hat{x}_{wo}$, null air mass flow rate $\hat{M}_a = 0$, vent coordinates ($x_o$,$y_o$ and $z_o$), and mass flow rate for each particle class $\hat{M}_{io}$. The latter is obtained from the total mass flow rate at inflow given the particle grain size distribution at the vent:

$$\hat{M}_{io} = f_{io}\hat{M}_o(1 - \hat{x}_{wo}) \qquad (16)$$

where $f_{io}$ is the mass fraction of class $i$ at the vent.

### 2.2 Entrainment coefficients

Turbulent entrainment of ambient air plays a key role on the dynamics of jets and buoyant plumes. In the basal region of volcanic columns, the rate of entrainment dictates if the volcanic jet enters into a collapse regime by exhaustion of momentum before the mixture becomes positively buoyant or if it evolves into a convective regime reaching much higher altitudes. Early laboratory experiments (e.g. Hewett et al., 1971) already indicated that the velocity of entrainment of ambient air is proportional to velocity differences parallel and normal to the plume axis (see inset in Fig. 1):

$$u_e = \alpha_s|\hat{u} - u_a\cos\theta| + \alpha_v|u_a\sin\theta| \qquad (17)$$

where $\alpha_s$ and $\alpha_v$ are dimensionless coefficients that control the entrainment along the stream-wise (shear) and cross-flow (vortex) directions respectively. Note that, in absence of wind (i.e. $u_a = 0$), the equation above reduces to $u_e = \alpha_s\hat{u}$ and the classical expression for entrainment velocity of Morton et al. (1956) is recovered. In contrast, under a wind field, both an along-plume (proportional to the relative velocity differences parallel to the plume) and a cross-flow (proportional to the wind normal component) contributions appear. However it is worth noting that Eq. (17) has not a solid theoretical justification and is used on empirical basis. A vast literature exists regarding the experimental (e.g. Dellino et al., 2014) and numerical (e.g. Suzuki and Koyaguchi, 2009)





Discussion Paper | Discussion Paper | Discussion Paper | Discussion Paper |

*integral*

determination of entrainment coefficients for jets and buoyant plumes. Based on these results, most 1-D ~~integrated~~ plume models available in literature consider: (i) same constant entrainment coefficients along the plume, (ii) pice-wise constant values at the different regions or, (iii) pice-wise constant values corrected by a factor $\sqrt{\hat{\rho}/\rho_a}$ (Woods, 1993). Typical values for the entrainment coefficients derived from experiments are of the order of $\alpha_s \approx 0.07$–$0.1$ for the jet region, $\alpha_s \approx 0.1$–$0.17$ for the buoyant region, and $\alpha_v \approx 0.3$–$1.0$ (e.g. Devenish, 2013). However, more recent experimental (Kaminski et al., 2005) and sensitivity analysis numerical studies (Charpentier and Espíndola, 2005) concluded that pice-wise constant functions are valid only as a first approach, implying that 1-D integrated models assuming constant entrainment coefficients do not always provide satisfactory results. This has also been corroborated by 3-D numerical simulations of volcanic plumes (Suzuki and Koyaguchi, 2013), which indicate that 1-D ~~integrated~~ models overestimate the effects of wind on turbulent mixing efficiency (i.e. the value of $\alpha_v$) and, consequently, underestimate plume heights under strong wind fields. For example, recent 3-D numerical simulation results for small-scale eruptions under strong wind fields suggest lower values of $\alpha_v$, in the range 0.1–0.3 (Suzuki and Koyaguchi, 2015). Based on experimental studies, Kaminski et al. (2005) and Carazzo et al. (2006, 2008a, b) proposed a parameterization for the shear entrainment coefficient $\alpha_s$ of jets and plumes as a function of the local Richardson number as:

*integral*

$$\alpha_s = 0.0675 + \left(1 - \frac{1}{A(z_s)}\right) Ri + \frac{r}{2}\frac{1}{A(z_s)}\frac{dA}{dz} \tag{18}$$

where $A(z_s)$ is an entrainment function depending on the dimensionless length $z_s = z/2r_o$ ($r_o$ is the vent radius) and $Ri = g(\rho_a - \hat{\rho})r/\rho_a \hat{u}^2$ is the Richardson number. In order to generalize to the case of two entrainment coefficient we modify such expression as:

$$\alpha_s = 0.0675 + \left(1 - \frac{1}{A(z_s)}\right) Ri \sin\theta + \frac{r}{2}\frac{1}{A(z_s)}\frac{dA}{dz} \tag{19}$$

*not explained or justified*





*not a sufficient motivation!*

Moreover in order to use a compact analytical expression and extend it to values of $z_s \le 10$ we fitted the experimental data of Carazzo et al. (2006, 2008b) considering the following function:

$$A(z_s) = c_o \frac{\left(z_s^2 + c_1\right)}{\left(z_s^2 + c_2\right)} \tag{20a}$$

*How is it justified? (see text for comments)*

$$\frac{1}{A(z_s)}\frac{dA}{dz} = \frac{1}{2r_0}\frac{2(c_2 - c_1)z_s}{\left(z_s^2 + c_1\right)\left(z_s^2 + c_2\right)} \tag{20b}$$

and in order to extrapolate to low $z_s$ we multiply $A(z_s)$ for the following function $h(z_s)$ that affects the behavior only for small values of $z_s$:

$$h(z_s) = \frac{1}{1 - c_4 \exp\left(-5\left(z_s/10 - 1\right)\right)} \tag{20c}$$

*report fit quality*

where $c_i$ are dimensionless fitting constants. Best-fit results and entrainment functions resulting from fitting Eqs. (20a)–(20c) are shown in Table 3 and Fig. 2 respectively. Finally, for the vortex entrainment coefficient $\alpha_v$, we adopt a parameterization proposed by Tate (2002) based on a few laboratory experiments:

$$\alpha_v = 0.34\left(\sqrt{2|Ri|}\frac{\bar{u}_a}{\hat{u}_o}\right)^{-0.125} \tag{21}$$

*An unpublished PhD thesis result...*

where $\hat{u}_o$ is the mixture velocity at the vent and $\bar{u}_a$ is the average wind velocity. For illustrative purposes, Fig. 3 shows the entrainment coefficients $\alpha_s$ and $\alpha_v$ predicted by Eqs. (19) and (21) for weak and strong plume cases under a prescribed wind profile.

### 2.3 Modeling of the umbrella region

The umbrella region is defined as the upper region of the plume, from about the NBL to the top of the column. This region can be dominated by processes of collapse of the mixture that reaches the top of the column, dissipating the excess of momentum at the NBL, and then collapsing as a gravity current (e.g. Woods and Kienle, 1994; Costa et al., 2013). The 1-D BPT should not be extended to this region because it assumes that the mixture still entrains air with the same mechanisms than below NBL and, moreover, predicts that the radius goes to infinity towards the top of the column. For these reasons, we describe the umbrella region adopting a semi-empirical approximation. We assume that the umbrella region extends from the NBL to the top of the column. Moreover, we consider that in the umbrella region air entrainment is null and the mixture is homogeneous, i.e. the content of air, water vapour, liquid water, ice, and total mass of particles do not vary with $z$.

*See text for comments.*

Pressure $P(z)$ is assumed equal to the atmospheric pressure $P_a(z)$ evaluated at the same level, whereas temperature decreases with $z$ due to the adiabatic cooling:

$$P(z) = P_a(z) \quad \text{and} \quad \frac{dT}{dP} = \frac{1}{\hat{c}\hat{\rho}} \tag{22}$$

As a consequence, the density of the mixture varies accordingly. The total height of the volcanic plume $H_t$, above the vent, is approximated as (e.g. Sparks, 1986):

$$H_t = 1.32(H_b + 8r_o) \tag{23}$$

*implies a constant entrainment coefficient (see text)*

where $H_b$ is the height of the Neutral Buoyancy Level (above the vent) and $r_o$ the radius at the vent. Between $H_b$ and $H_t$, the coordinates $x$ and $y$ of the position of the plume centre and the plume radius $r$ are parameterized as a function of the elevation $z$, with $H_b \leq z \leq H_t$. The position of the plume centre is assumed to vary linearly with the same slope at the NBL, whereas the effective plume radius is assumed to decrease as a Gaussian function:

$$x = x_b + (z - H_b) \left. \frac{dx}{dz} \right|_{z=z_b} \tag{24}$$

$$y = y_b + (z - H_b) \left. \frac{dy}{dz} \right|_{z=z_b} \tag{25}$$



$$r = r_b e^{-(z-H_b)^2/2\sigma_H^2} \tag{26}$$

where $x_b$, $y_b$, $r_b$ are, respectively, the coordinates $x$ and $y$ of the center of the plume and the plume radius at the NBL, and $\sigma_H = H_t - H_b$.

Finally, assuming that the kinetic energy of the mixture is converted to potential energy, the vertical velocity is approximated to decrease as the square root of the distance from the NBL:

$$u_z = u_{zb} \sqrt{\frac{H_t - z}{H_t - H_b}} \tag{27}$$

where $u_{zb}$ is the vertical velocity of the plume at the NBL.

## 3 Plume wet aggregation model

Particle aggregation can occur inside the column or in the ash cloud during subsequent atmospheric dispersion (e.g. Carey and Sigurdsson, 1982; Durant et al., 2009), thereby affecting the sedimentation dynamics and deposition of volcanic ash. Our model explicitly accounts for aggregation in the plume by adding source ($A_i^+$) and sink ($A_i^-$) terms for aggregates and aggregated particles in their respective particle mass balance Eq. (2g) and by modifying the settling velocity of the aggregates. Given the complexity of aggregation phenomena, not yet fully understood, we consider only the occurrence of wet aggregation and neglect dry aggregation mechanisms driven by electrostatic forces or disaggregation processes resulting from particle collisions that can break and decompose aggregates. Costa et al. (2010) and Folch et al. (2010) proposed a simplified wet aggregation model in which particles aggregate on a single effective aggregated class characterized by a diameter $d_A$ (i.e. aggregation only involves particle classes having an effective diameter smaller than $d_A$, typically in the range 100–300 µm). Under this




Discussion Paper | Discussion Paper | Discussion Paper | Discussion Paper |

simplifying assumption it follows that:

$$A_i^+ = \left(\sum A_j^-\right)\delta_{ik} \tag{28}$$

*notation is unclear (indexes do not match)*

where $k$ is the index of the aggregated class and the sum over $j$ spans all particle classes having diameters lower than $d_\mathrm{A}$. The mass of particles of class $i$ ($d_i < d_\mathrm{A}$) that aggregate per unit of time and length in a given plume cross-section is:

$$A_i^- = \dot{n}_i\left(\rho_{\mathrm{p}i}\frac{\pi}{6}d_i^3\right)\pi r^2 \tag{29}$$

where $\dot{n}_i$ is the number of particles of class $i$ that aggregate per unit volume and time, estimated as:

$$\dot{n}_i \approx \frac{\dot{n}_\mathrm{tot}N_i}{\sum N_j} \tag{30}$$

In the expression above, $N_i$ is the number of particles of diameter $d_i$ in an aggregate of diameter $d_\mathrm{A}$, and $\dot{n}_\mathrm{tot}$ is the total particle decay per unit volume and time. Costa et al. (2010) considered that $N_i$ is given by a semi-empirical fractal relationship (e.g. Jullien and Botet, 1987; Frenklach, 2002; Xiong and Friedlander, 2001):

$$N_i = k_\mathrm{f}\left(\frac{d_\mathrm{A}}{d_i}\right)^{D_\mathrm{f}} \tag{31}$$

where $k_\mathrm{f}$ is a fractal pre-factor and $D_\mathrm{f}$ is the fractal exponent. Costa et al. (2010); Folch et al. (2010) assumed constant values for $k_\mathrm{f}$ and $D_\mathrm{f}$ that where calibrated by best-fitting tephra deposits from 18 May 1980 Mount St. Helens and 17–18 September 1992 Crater Peak eruptions. However, for the granulometric data from these deposits they used a cut-off considering only particles larger than about 10 µm, for which the gravitational aggregation kernel dominates. This poses a problem if one wants to extend the granulometric distribution to include micrometric and sub-micrometric particles, for which





the Brownian kernel is the dominant one (it is known that Brownian particle-particle interaction has typical values of $D_\mathrm{f} \approx 2$, with values ranging between 1.5 and 2.5, e.g. Xiong and Friedlander, 2001). Actually, preliminary model tests involving micrometric and sub-micrometric particle classes considering constant values for $D_\mathrm{f}$ and $k_\mathrm{f}$ have revealed a strong dependency of results (fraction of aggregated mass) on both granulometric cut-off and bin width (particle grain size discretization). In order to overcome this problem, we assume a size-dependent fractal exponent as:

$$D_\mathrm{f}(d) = D_\mathrm{fo} - \frac{a\left(D_\mathrm{fo} - D_\mathrm{min}\right)}{1 + \exp((d - d_\mu)/d_\mu)} \tag{32}$$

where $D_\mathrm{fo} \le 3$, $D_\mathrm{min} = 1.6$, $d_\mu \approx 2$ µm, and $a = 1.36788$. The values of $D_\mathrm{min}$ and $d_\mu$ represent, respectively, the minimum value of $D_\mathrm{f}$ relevant for sub-micrometric particles and the scale below which the Brownian aggregation kernel becomes dominant. For the fractal pre-factor $k_\mathrm{f}$ we adopt the expression of Gmachowski (2002):

$$k_\mathrm{f} = \left[\sqrt{1.56 - \left(1.728 - \frac{D_\mathrm{f}}{2}\right)^2} - 0.228\right]^{D_\mathrm{f}}\left(\frac{2 + D_\mathrm{f}}{D_\mathrm{f}}\right)^{D_\mathrm{f}/2} \tag{33}$$

Figure 4 shows the values of $D_\mathrm{f}(d)$ and $k_\mathrm{f}(d)$ predicted by Eqs. (32) and (33) for a range of $D_\mathrm{fo}$. We have performed different tests to verify that, in this way, the results of the aggregation model become much more robust independently of the distribution cut-off ($\Phi_\mathrm{min} = 8, 10, 12$) and bin width ($\Delta\Phi = 1, 0.5, 0.25$), with maximum differences in the aggregated mass laying always below 10 %.

The total particle decay per unit volume and time $\dot{n}_\mathrm{tot}$ is given by:

$$\dot{n}_\mathrm{tot} = \hat{f}\alpha_m\left(A_\mathrm{B}n_\mathrm{tot}^2 + A_\mathrm{TI}\phi^{4/D_\mathrm{f}}n_\mathrm{tot}^{2-4/D_\mathrm{f}} + A_\mathrm{S}\phi^{3/D_\mathrm{f}}n_\mathrm{tot}^{2-3/D_\mathrm{f}} + A_\mathrm{DS}\phi^{4/D_\mathrm{f}}n_\mathrm{tot}^{2-4/D_\mathrm{f}}\right) \tag{34}$$

where $\alpha_m$ is a mean (class-averaged) sticking efficiency, $\phi$ is the solid volume fraction, $n_\mathrm{tot}$ is the total number of particles per unit of volume that can potentially ~~participate~~ *aggregate*

~~to the aggregation~~ and $\hat{f}$ is a correction factor that accounts for conversion from gaussian to top-hat formalism (see Appendix A for details). The expression above comes from integrating the collection kernel over all particle sizes, and involves the product of the (averaged) sticking efficiency times the collision frequency function accounting for Brownian motion ($A_\mathrm{B}$), collision due to turbulence as result of inertial effects ($A_\mathrm{TI}$), laminar and turbulent fluid shear ($A_\mathrm{S}$), and differential sedimentation ($A_\mathrm{DS}$). The term $A_\mathrm{B}$ derives from the Brownian collision kernel $\beta_{B,ij}$ (~~e.g.~~ Costa et al., 2010):

$$\beta_{B,ij} = \frac{2k_\mathrm{b}\hat{T}}{3\hat{\mu}}\frac{(d_i + d_j)^2}{d_j d_j} \tag{35}$$

where $k_\mathrm{b}$ is the Boltzmann constant and $\hat{\mu}$ is the mixture dynamic viscosity (≈ air viscosity at the bulk temperature $\hat{T}$). The term $A_\mathrm{TI}$ derives from the collision kernel due to turbulence as result of inertial effects $\beta_{\mathrm{TI},ij}$ (e.g. Pruppacher and Klett, 1996; Jacobson, 2005):

$$\beta_{\mathrm{TI},ij} = \frac{\epsilon^{3/4}}{g\hat{\nu}^{1/4}}\frac{\pi}{4}(d_i + d_j)^2|u_{\mathrm{s}j} - u_{\mathrm{s}i}| \tag{36}$$

where $\hat{\nu}$ is the mixture kinematic viscosity and $\epsilon$ is the dissipation rate of turbulent kinetic energy, computed assuming the Smagorinsky–Lilly model:

$$\epsilon = 2\sqrt{2}k_\mathrm{s}^2\frac{\hat{u}^3}{r} \tag{37}$$

where $k_\mathrm{s} \approx 0.1$–$0.2$ is the constant of Smagorinsky. The term $A_\mathrm{S}$ derives from the collision kernel due to laminar and turbulent fluid shear $\beta_{\mathrm{S},ij}$ (~~e.g.~~ Costa et al., 2010):

$$\beta_{\mathrm{S},ij} = \frac{\Gamma_\mathrm{S}}{6}(d_i + d_j)^3 \tag{38}$$





where $\Gamma_\mathrm{S}$ is the fluid shear, computed as:

$$\Gamma_\mathrm{S} = \max\left(\left|\frac{\mathrm{d}\hat{u}}{\mathrm{d}r}\right|, \left(\frac{\epsilon}{\nu}\right)^{1/2}\right) \tag{39}$$

Finally, the term $A_\mathrm{DS}$ derives from the differential sedimentation collision kernel $\beta_{\mathrm{DS},ij}$ (e.g. Costa et al., 2010):

$$\beta_{\mathrm{DS},ij} = \frac{\pi}{4}(d_i + d_j)^2|u_{\mathrm{s}i} - u_{\mathrm{s}j}| \tag{40}$$

where $u_{\mathrm{s}i}$ denotes the settling velocity of particle class $i$. Note that, with respect the original formulation of Costa et al. (2010), using the same approach and approximation, we have included the additional term $A_\mathrm{TI}$ due to the turbulent inertial kernel that, thanks to the similarity between Eqs. (40) and (36), can be easily derived. Once these kernels are integrated, expressions for the terms in Eq. (34) yield:

*Please report the integration formula*

$$A_\mathrm{B} = -\frac{4k_\mathrm{b}\hat{T}}{3\hat{\mu}} \tag{41a}$$

$$A_\mathrm{S} = -\frac{2}{3}\Gamma_\mathrm{S}\xi^3 \tag{41b}$$

$$A_\mathrm{DS} = -\frac{\pi(\rho_\mathrm{p} - \hat{\rho})g\xi^4}{48\hat{\mu}} \tag{41c}$$

$$A_\mathrm{TI} = 1.82\frac{\epsilon^{3/4}}{g\nu^{1/4}}A_\mathrm{DS} \tag{41d}$$

where $\xi = d_j v_j^{-1/D_\mathrm{f}}$ is the diameter to volume fractal relationship and $v_j$ is the particle volume. Note that for spherical particles in the Euclidean space ($D_\mathrm{f} = 3$) $v_j = \pi d_j^3/6$ and $\xi = (6/\pi)^{1/3}$.

The total number of particles per unit of volume available for aggregation is related to particle class mass concentration at each section of the plume $\hat{C}_j$ and can be estimated as (see Appendix B):

$$n_{\mathrm{tot}} = \frac{1}{3\log 2}\sum_j \left(\frac{6\hat{C}_j}{\pi \Delta \Phi_j \rho_{\mathrm{p}j}}\right)\left[\frac{1}{d_{\mathrm{a}j}^3} - \frac{1}{d_{\mathrm{b}j}^3}\right] \tag{42}$$

where $d_{\mathrm{a}j}$ and $d_{\mathrm{b}j}$ are the particle diameters of the limits of the interval $j$ and:

$$\hat{C}_j = \hat{\rho}\frac{\hat{M}_j}{\hat{M}} \tag{43}$$

\rho should probably be removed

Finally, the class-averaged sticking efficiency $\alpha_m$ appearing in (34) is computed as:

$$\alpha_m = \frac{\sum_i \sum_j f_i f_j \alpha_{ij}}{\sum_i \sum_j f_i f_j} \tag{44}$$

where $f_k$ is the particle class mass fraction, and $\alpha_{ij}$ is the sticking efficiency between the classes $i$ and $j$. In presence of a pure ice phase we assume that ash particles stick as ice particles ($\alpha_m = 0.09$). In contrast, in presence of a liquid phase, the aggregation model considers:

$$\alpha_{ij} = \frac{1}{1 + (\mathrm{St}_{ij}/\mathrm{St}_{\mathrm{cr}})^q} \tag{45}$$

where $\mathrm{St}_{\mathrm{cr}} = 1.3$ is the critical Stokes number, $q = 0.8$ is a constant, and $\mathrm{St}_{ij}$ is the Stokes number based on the binder liquid (water) viscosity:

$$\mathrm{St}_{ij} = \frac{8\hat{\rho}}{9\mu_{\mathrm{l}}}\frac{d_i d_j}{d_i + d_j}|u_i - u_j| \tag{46}$$





where

$$|u_i - u_j| = |u_{\mathrm{s}i} - u_{\mathrm{s}j}| + \frac{8k_{\mathrm{b}}\hat{T}}{3\hat{\mu}\pi d_i d_j} + \frac{2\Gamma_{\mathrm{s}}(d_i + d_j)}{3\pi} \tag{47}$$

Obviously, our aggregation model requires the presence of water either in liquid or solid phases, i.e. aggregation will only occur in ~~these~~ regions of the plume where water vapor (of magmatic origin or entrained by moist air) meets condensation/deposition conditions. This depends on complex relationships between plume dynamics and ambient conditions. For high-intensity (strong) plumes having high values of $\hat{M}$, the condition $P_{\mathrm{v}} \geq e_{\mathrm{l}}$ when $\hat{T} > T_{\mathrm{f}}$ is rarely meet, implying no formation of a liquid water window within the plume. Aggregation occurs in this case only at the upper parts of the column, under the presence of ice. In contrast, lower-intensity (weak) plumes having lower values of $\hat{M}$ can form a liquid water window if the term $M_{\mathrm{a}}$ dominates in Eq. (5). However, this also depends on a complex balance between air entrainment efficiency, ambient moisture, plume temperature, height level, cooling rate and ambient conditions. Aggregation by liquid water is much favored under moist environments and by efficient air entrainment. Note that, keeping all eruptive parameters constant, the occurrence (or not) of wet aggregation by liquid water can vary with time depending on fluctuations of the atmospheric moisture and wind intensity along the day.

those

(Please specify a range)

In summary, the solution of the aggregation model embedded in FPLUME-1.0 consists on the following steps:

I would move this paragraph in the code description section.
The algorithm should be described in more detail (see text for comments)

1. At each section of the plume, determine the water vapor condensation or deposition conditions depending on $\hat{T}$ and $P_{\mathrm{v}}$ using Eq. (8) or Eq. (9) respectively.

2. In case of saturation or deposition, compute the class-averaged sticking efficiency $\alpha_m$ for liquid water or ice using Eq. (44).

3. Estimate the total number of particles per unit of volume available for aggregation $n_{\mathrm{tot}}$ depending on $\hat{C}_j$ using Eq. (42).

4. Compute the integrated aggregation kernels using Eq. (41a) to (41d).
5. Compute the total particle decay per unit volume and time $\dot{n}_{tot}$ using Eq. (34) depending also on the solid volume fraction.
6. Compute the number of particles of diameter $d_i$ in an aggregate of given diameter $d_A$ using Eq. (31) assuming size-dependent fractal exponent $D_f$ and pre-factor $k_f$.
7. Compute class particle decay $\dot{n}_i$ using Eq. (30).
8. Finally, compute the mass sink term for each aggregating class $A_i^-$ using Eq. (29) and the mass source term $A_i^+$ for the aggregated class using Eq. (28) to introduce these terms in the particle class mass balance equations (2g).

## 4 FPLUME-1.0

We solve the model equations using FPLUME-1.0, a code written in FORTRAN90 that uses the LSODE library (Hindmarsh, 1980) to solve the set of first order ordinary differential equations. Model inputs are eruption start and duration (different successive eruption phases can be considered), vent coordinates ($x_o$,$y_o$) and elevation ($z_o$), conditions at the vent (exit velocity $\hat{u}_o$, magma temperature $\hat{T}_o$, magmatic water mass fraction $\hat{w}_o$, and total grain size distribution) and total column height $H_t$ or mass eruption rate $\hat{M}_o$. The code has two solving modes. If $\hat{M}_o$ is given, the code solves directly for $H_t$. On the contrary, if $H_t$ is given, the code solves iteratively for $\hat{M}$. Wind profiles can be furnished in different formats, including standard atmosphere, atmospheric soundings, and profiles extracted from meteorological re-analysis datasets. If the aggregation model is switched on, additional inputs are required including size and density of the aggregated class, aggregates settling velocity factor (to account for the decrease in settling velocity of aggregates due to increase in porosity), and fractal exponent for coarse particles $D_{fo}$. The rest of parameters (e.g. specific heats, the value of the constant $\chi$ for particle fallout probability, parameterization of the entrainment coefficients,





etc.) have assigned default values but can be modified by the user using a configure file.

Model outputs include a text file with the results for each eruption phase giving values of all computed variables (e.g. $\hat{u}$, $\hat{T}$, $\hat{\rho}$, etc.) at different heights, and a file ~~given~~ *giving* the mass flow rate of each particle class that falls from the column at different heights (cross-sections). This file provides the phase-dependent source term, and hence serves to couple FPLUME with atmospheric dispersion models. In case of wet aggregation, the effective granulometry predicted by the aggregation model is also provided.

## 5 Test cases

As we mentioned above, here we apply FPLUME to two eruptions relatively well characterized by previous studies. In particular we consider the strong plume formed during 4 April 1982 by El Chichón 1982 eruption (e.g. Sigurdsson et al., 1984; Bonasia et al., 2012) and the weak plume formed during the 6 May 2010 Eyjafjallajökull eruption (e.g. Bonadonna et al., 2011; Folch, 2012).

### 5.1 Phase-B El Chichón 1982 eruption

El Chichón volcano reawakened in 1982 with three significant Plinian episodes occurring during 29 March (phase A) and 4 April (phases B and C). Here we focus on the second major event, starting at 01:35 UTC on 4 April and lasting nearly 4.5 h (Sigurdsson et al., 1984). Bonasia et al. (2012) used analytical (HAZMAP) and numerical (FALL3D) tephra transport models to reconstruct ground deposit observations for the three main eruption fallout units. Deposit best-fit inversion results for phase-B suggested column heights between 28 and 32 km (above vent level, a.v.l.) and a total erupted mass ranging between $2.2 \times 10^{12}$ and $3.7 \times 10^{12}$ kg. Considering a duration ~~on~~ *of* 4.5 h, the resulting averaged mass eruption rates are between $1 \times 10^8$ and $2.3 \times 10^8$ kg s$^{-1}$. TGSD of phases B and C were estimated by Rose and Durant (2009) weighting by mass, by isopach volume and using the Voronoi method. Bonasia et al. (2012) found that the reconstruction of the deposits is reasonably achieved taking into account the empirical Cornell aggregation parameterization (Cornell et al., 1983). In this simplistic approach, 50 % of the 63–44 µm ash, 75 % of the 44–31 µm ash and 100 % of the less than 31 µm ash are assumed to aggregate as particles with a diameter of 200 µm and density of 200 kg m$^{-3}$. Note that here, as in previous studies (Folch et al., 2010), we use a modified version of Cornell et al. (1983) parameterization that assumes that 90 % and not 100 % of the particle smaller than 31 µm fall as aggregates.

We use this test case to verify whether FPLUME can reproduce results from these previous studies and the results of our aggregation model are, in this case, consistent with those of Cornell et al. (1983) parameterization. Input values for FPLUME are summarized in Table 4. We used the TGSD of Rose and Durant (2009) with 17 particle classes ranging from 64 mm (Φ = −6) to 1 µm (Φ = 10). The wind profile has been obtained from the University of Wyoming soundings database (weather.uwyo.edu/upperair/sounding.html) for 4 April 1982 at 00:00 UTC at the station number 76 644 (lon=-89.65, lat=20.97). Figure 5 shows the wind profile and the FPLUME results for bulk velocity and plume radius. The model predicts a total plume height of 28 km (a.s.l.), a mass eruption rate of $2.7 \times 10^8$ kg s$^{-1}$, and a total erupted mass of $4.4 \times 10^{12}$ kg. These values are consistent but slightly higher than those from previous studies (Bonasia et al., 2012). Regarding the aggregation model, we did several sensitivity runs to look into the impact of the fractal exponent $D_{fo}$ on the fraction of aggregates, ranging this parameter between 2.85 and 3.0 at 0.01 steps values (see Fig. 6). As anticipated in the original formulation (Costa et al., 2010; Folch et al., 2010), the results of the aggregation model are sensitive to this parameter. Values of $D_{fo} = 2.96$ fit very well the total mass fraction of aggregates predicted by Cornell but not the fraction of the aggregating classes (Fig. 7 a). In contrast, we find a more reasonable fit with $D_{fo} = 2.92$, although in this case the relative differences for the total mass fraction of aggregates are of about 15 %, with our model under-predicting with respect to Cornell (Fig. 7b).

*Are these values inverted?*





A clear advantage of a physical aggregation model of ash particles inside the eruption column, with respect an empirical parameterization like that of Cornell et al. (1983), is that allows to estimate the fraction of very fine ash that escapes to aggregation processes and is transported distally within the cloud. As we mentioned above, based on the features of the observed deposits, Cornell et al. (1983) proposed that 100 % of particles smaller than 31 µm fall as aggregates that is quite reasonable as most of fine ash falls prematurely. However assessing the small mass fraction of fine ash that escapes to aggregation processes is crucial for aviation risk mitigation and for comparing model simulations with satellite observations. For example, in the case of El Chichón 1982 eruption, for $D_{fo} = 2.92$, the model predicts that ≈ 10 % of fine ash between 20 and 2 µm in diameter escapes to aggregation processes. This value is an order of magnitude larger than that estimated by Schneider et al. (1999) using TOMS and AVHRR but we need to consider that we do not account for dry aggregation that can be dominant for very fine particles.

*it*

### 5.2 6 May 2010 Eyjafjallajökull eruption phase

The infamous April–May 2010 Eyjafjallajökull eruption, that disrupted the European North Atlantic region airspace (e.g. Folch, 2012), was characterized by a very pulsating behavior, resulting ~~on~~ a nearly continuous production of weak plumes that oscillated in height between 2 and 10 km (a.s.l.) along the 39 day-long eruption (e.g. Gudmundsson et al., 2012). During 4–8 May, Bonadonna et al. (2011) performed in-situ observations of tephra accumulation rates and PLUDIX Doppler radar measurements of settling velocities at different locations which then used to determine erupted mass, mass eruption rates and grain size distributions. The authors estimated a TGSD representative of 30 min of eruption by combining ground-based grain-size observations (using a Voronoi tessellation technique) and ash mass retrievals (7–9Φ particles) from MSG-SEVIRI satellite imagery for 6 May between 11:00 and 11:30 UTC. On the other hand, they also report the in-situ observation of sedimentation of dry and wet aggregates falling as particle clusters and poorly structured and liquid accretionary pellets

*in*

(AP1 and AP3 according to Brown et al., 2012, nomenclature). Bonadonna et al. (2011) did also grain-size analyses of collected aggregates using scanning electron microscope (SEM) images. The combination of all these data allowed them to determine how the original TGSD was modified by the formation of different types of aggregates (see Fig. 8). The total mass fraction of aggregates was estimated to be about 25 % with aggregate sizes ranging between 1Φ (500 µm) and 4Φ (62.5 µm). These results constitute a rare and valuable dataset to test the aggregation model implemented in FPLUME. However, several challenges can be anticipated. First, our model assumes a single aggregated class and, as a consequence, we can expect to reproduce only the total mass fraction of aggregates, but not to match the resulting mass fraction distribution class by class. Second, the proportion of dry vs. wet aggregates is unknown and, moreover, wet aggregation could have occurred within the plume but also by local rain showers that scavenged coarse particles (Bonadonna et al., 2011). For these reasons, we aim to capture the correct order of magnitude of total mass fraction of ash that went into aggregates.

*Move below*

Input values for FPLUME are summarized in Table 5. The wind profile (see Fig. 9) was extracted from the ERA-Interim re-analysis dataset interpolating values at the vent coordinates. Preliminary simulations using time-averaged plume heights of 3.5–4.5 km (a.v.l.) did not result in formation of aggregates because the model did not predict the existence of a liquid water window nor the formation of ice. However, on short time scales these plume heights can be very different from the daily (hourly) time-averaged values. In fact, Arason et al. (2011) determined 5 min time series of the echo top radar data of the eruption plume altitude and for 6 May they observed oscillations between 3.5 and 8.5 km (a.v.l). This is consistent with Gudmundsson et al. (2012), which for 6 May reported a median plume height of 4 km (a.v.l.) and a maximum elevation of around 8 km (a.v.l). This may suggest that wet aggregates could have formed within the plume not continuously but during sporadic higher-intensity column pulses. In order to check this possibility, we performed a parametric study to compute the total mass fraction of formed wet aggregates depending on the column height. As shown

*Please specify the ranges of varied parameters*



*(move first sentence here)*

in Fig. 10, 10 % in mass of wet aggregates is predicted by our model only for column heights ranging between 6.7 and 7.5 km (a.v.l.). For the considered input parameters, model entrainment parameterizations, and ambient conditions (wind and moisture profile), we only observed the formation of a window in the plume containing liquid water for plume altitudes above 5.8 km (a.v.l.). For illustrative purposes, Fig. 11 shows the resulting grain size distribution for a column height of 7 km (a.v.l.) and two different values of the fractal exponent $D_f$. As anticipated, the model can predict the total mass fraction of aggregates, but an error (< 10 %) exists for some particular classes.

## 6 Conclusions

We presented FPLUME, a 1-D cross-section averaged volcanic plume model based on the BPT that accounts for plume bent over by wind, entrainment of ambient moisture, effects of water phase changes, particle fallout and re-entrainment, a new parameterization for the air entrainment coefficients and an ash wet aggregation model based on Costa et al. (2010). Given conditions at the vent (mixture exit velocity, temperature and magmatic water content) and a wind profile, the model can solve for plume height given the eruption rate or vice-versa. FPLUME can also be extended above the NBL, i.e. to solve the umbrella region semi-empirically in case of strong plumes. In case of favorable wet aggregation conditions (formation of a liquid water window inside the plume or in presence of ice at the upper regions), the aggregation model predicts an "effective" grain size distribution considering a single aggregated class. We have tested the model implementation simulating well-studied eruptions (results not shown here) obtaining good agreements. For the aggregation model, two test cases have been considered, the Phase-B of El Chichón 1982 eruption and the 6 May 2010 Eyjafjallajökull eruption phase. For the first case, we got reasonable agreement with the empirical Cornell parameterization using a fractal exponent of $D_{fo} = 2.92$, with wet aggregation occurring under the presence of ice (as expected for large strong plumes). For the second case, we could reproduce the observed total mass fraction of aggre-

*It is not clear whether this tests are those described in the sections above. If not, this sentence should be removed.*





Discussion Paper | Discussion Paper | Discussion Paper | Discussion Paper |

gates for plume heights between 6.7 and 8.5 km (a.v.l.). Wet aggregation occurs in this case within a narrow window where conditions for liquid water to form are met. In case of aggregation, results are sensitive to the fractal exponent, which may range from $D_{fo} = 2.92$ to $D_{fo} = 2.99$. Future studies are necessary to better understand and constrain the role of this parameter.

**Code availability**

The code FPLUME-1.0 is available under request for research purposes.

## Appendix A: Correction factor $f$ for mass distribution for top-hat vs. Gaussian formalism

Denoting with $R$ the top-hat radius of the plume and with $b$ the Gaussian length scale the relationship between them can be written as (e.g. Davidson, 1986):

$$b^2 = R^2/2 \tag{A1}$$

Assuming a Gaussian profile for the concentration, $C(r)$, the mean value between $r = 0$ (where the concentration is maximum) and $r = R$ is:

$$\langle C \rangle = C_0/R^2 \int_0^\infty r \exp\left(-r^2/b^2\right) \mathrm{d}r = C_0/(2b^2) \int_0^\infty r \exp\left(-r^2/b^2\right) \mathrm{d}r = 0.25 C_0 \tag{A2}$$

that implies $\hat{C} = 0.25C_0$. Following similar calculations we have also:

$$\langle C^2 \rangle = C_0^2/R^2 \int_0^\infty r \exp\left(-2r^2/b^2\right) \mathrm{d}r = C_0^2/(2b^2) \int_0^\infty r \exp\left(-2r^2/b^2\right) \mathrm{d}r = 0.125 C_0^2 \tag{A3}$$



$$\langle C^3 \rangle = C_0^3/R^2 \int_0^\infty r \exp\left(-3r^2/b^2\right) \mathrm{d}r = C_0^3/(2b^2) \int_0^\infty r \exp\left(-3r^2/b^2\right) \mathrm{d}r = 0.0833 C_0^3 \tag{A4}$$

Therefore if we use average (top-hat) variables in Eq. (34) we need to keep in mind that concentration appears in the nonlinear terms and therefore we should use the following correction factors:

$$\hat{f}_2 = \frac{\langle C^2 \rangle}{\hat{C}^2} = \frac{0.125 C_0^2}{(0.25 C_0)^2} = \frac{0.125 C_0^2}{0.0625 C_0^2} = 2 \tag{A5}$$

$$\hat{f}_3 = \frac{\langle C^3 \rangle}{\hat{C}^3} = \frac{0.0833 C_0^2}{0.015625 C_0^3} = 5.33 \tag{A6}$$

and so on ($\langle \cdot \rangle$ denotes the average using the top-hat filter, e.g. $\hat{C} = \langle C \rangle$). Because terms in Eq. (34) scale with concentration with a power of two we need to account for a correction factor $\hat{f} = \hat{f}_2$. The factor $\hat{f}$ can be also used to correct underestimation of Eulerian time scale with respect Lagrangian time scale (e.g. Dosio et al., 2005).

## Appendix B: Computation of $n_{tot}$

Consider a particle grain size distribution discretized in $n$ bins of width $\Delta\Phi_j$ with the bin center at $\Phi_j$ and where $\Phi_{ja}$ and $\Phi_{jb}$ are the bin limits (i.e. $\Delta\Phi_j = \Phi_{jb} - \Phi_{ja}$). The number of particles per unit volume in the bin $\Phi_j$ (assuming spherical particles) is:

$$n(\Phi_j) = \int_{\Phi_{ja}}^{\Phi_{jb}} \frac{6C(\Phi)}{\pi \rho(\Phi) d^3(\Phi)} \mathrm{d}\Phi \tag{B1}$$

Considering that $d(\Phi) = d_* 2^{-\Phi} = d_* e^{-\Phi \log 2}$ and the top-hat formalism, the above expression can be approached as:

$$n(\Phi_j) \approx \frac{6\hat{C}_j}{\pi \rho_j d_*^3 \Delta\Phi_j} \int_{\Phi_{ja}}^{\Phi_{jb}} e^{3\Phi \log 2} \mathrm{d}\Phi = \frac{1}{3 \log 2} \left( \frac{6\hat{C}_j}{\pi \rho_j d_*^3 \Delta\Phi_j} \right) \left[ e^{3 \log 2 \Phi_{jb}} - e^{3 \log 2 \Phi_{ja}} \right] \tag{B2}$$

Adding the contribution of all bins, this yields to:

$$n_{\mathrm{tot}} = \frac{1}{3 \log 2 d_*^3} \sum_j \left( \frac{6\hat{C}_j}{\pi \rho_j \Delta\Phi_j} \right) \left[ e^{3 \log 2 (\Phi_j + \Delta\Phi_j/2)} - e^{3 \log 2 (\Phi_j - \Delta\Phi_j/2)} \right] \tag{B3}$$

or, in terms of particle diameter:

$$n_{\mathrm{tot}} = \frac{1}{3 \log 2} \sum_j \left( \frac{6\hat{C}_j}{\pi \Delta\Phi_j \rho_j} \right) \left[ \frac{1}{d_{\mathrm{a}j}^3} - \frac{1}{d_{\mathrm{b}j}^3} \right] \tag{B4}$$

which is Eq. (42).

*Acknowledgements.* This work was partially supported by the MED-SUV Project funded by the European Union (FP7 Grant Agreement n.308665). We thank C. Bonadonna for providing grain size data for the Eyjafjallajökull test case.

## References

Arason, P., Petersen, G. N., and Bjornsson, H.: Observations of the altitude of the volcanic plume during the eruption of Eyjafjallajökull, April–May 2010, Earth Syst. Sci. Data, 3, 9–17, doi:10.5194/essd-3-9-2011, 2011. 8035





Arastoopour, H., Wang, C., and Weil, S.: Particle-particle interaction force in a dilute gas-solid system, Chem. Eng. Sci., 37, 1379–1386, doi:10.1016/0009-2509(82)85010-0, 1982. 8019

Bonadonna, C., Genco, R., Gouhier, M., Pistolesi, M., Cioni, R., Alfano, F., Hoskuldsson, A., and Ripepe, M.: Tephra sedimentation during the 2010 Eyjafjallajökull eruption (Iceland) from deposit, radar, and satellite observations, J. Geophys. Res.-Sol. Ea., 116, 2156–2202, doi:10.1029/2011JB008462, b12202, 2011. 8032, 8034, 8035, 8059, 8062

Bonasia, R., Costa, A., Folch, A., Macedonio, G., and Capra, L.: Numerical simulation of tephra transport and deposition of the 1982 El Chichón eruption and implications for hazard assessment, J. Volcanol. Geoth. Res., 231–232, 39–49, doi:10.1016/j.jvolgeores.2012.04.006, 2012. 8032, 8033

Brown, R., Bonadonna, C., and Durant, A.: A review of volcanic ash aggregation, volcanic ash: an agent in Earth systems, Phys. Chem. Earth, 45–46, 65–78, doi:10.1016/j.pce.2011.11.001, 2012. 8012, 8035

Bursik, M.: Effect of wind on the rise height of volcanic plumes, Geophys. Res. Lett., 28, 3621–3624, doi:10.1029/2001GL013393, 2001. 8012, 8015, 8019, 8048

Carazzo, G., Kaminski, E., and Tait, S.: The route to self-similarity in turbulent jets and plumes, J. Fluid Mech., 547, 137, doi:10.1017/S002211200500683X, 2006. 8021, 8022, 8049, 8053

Carazzo, G., Kaminski, E., and Tait, S.: On the dynamics of volcanic columns: a comparison of field data with a new model of negatively buoyant jets, J. Volcanol. Geoth. Res., 178, 94–103, doi:10.1016/j.jvolgeores.2008.01.002, 2008a. 8021

Carazzo, G., Kaminski, E., and Tait, S.: On the rise of turbulent plumes: quantitative effects of variable entrainment for submarine hydrothermal vents, terrestrial and extra terrestrial explosive volcanism, J. Geophys. Res., 113, B09201, doi:10.1029/2007JB005458, 2008b. 8021, 8022

Carey, S. N. and Sigurdsson, H.: Influence of particle aggregation on deposition of distal tephra from the May 18, 1980, eruption of Mount St. Helens volcano, J. Geophys. Res.-Sol. Ea., 87, 7061–7072, doi:10.1029/JB087iB08p07061, 1982. 8024

Charpentier, I., and Espíndola, J. M.: A study of the entrainment function in models of Plinian columns: characteristics and calibration, Geophys. J. Int., 160, 1123–1130, doi:10.1111/j.1365-246X.2005.02541.x, 2005. 8021

Cornell, W., Carey, S., and Sigurdsson, H.: Computer simulation of transport and deposition of the campanian Y-5 ash, explosive Volcanism, J. Volcanol. Geoth. Res., 17, 89–109, doi:10.1016/0377-0273(83)90063-X, 1983. 8033, 8034

Costa, A., Macedonio, G., and Folch, A.: A three-dimensional Eulerian model for transport and deposition of volcanic ashes, Earth Planet. Sc. Lett., 241, 634–647, 2006. 8015, 8019

Costa, A., Folch, A., and Macedonio, G.: A model for wet aggregation of ash particles in volcanic plumes and clouds: 1. Theoretical formulation, J. Geophys. Res.-Sol. Ea., 115, B09201, doi:10.1029/2009JB007175, 2010. 8012, 8024, 8025, 8027, 8028, 8033, 8036, 8046

Costa, A., Folch, A., and Macedonio, G.: Density-driven transport in the umbrella region of volcanic clouds: implications for tephra dispersion models, Geophys. Res. Lett., 40, 4823–4827, doi:10.1002/grl.50942, 2013. 8011, 8023

Davidson, G. A.: Gaussian versus top-hat profile assumptions in integral plume models, Atmos. Environ., 20, 417–478, 1986. 8037

Degruyter, W. and Bonadonna, C.: Improving on mass flow rate estimates of volcanic eruptions, Geophys. Res. Lett., 39, 16, doi:10.1029/2012GL052566, 2012. 8011, 8012

Dellino, P., Mele, D., Bonasia, R., Braia, G., La Volpe, L., and Sulpizio, R.: The analysis of the influence of pumice shape on its terminal velocity, Geophys. Res. Lett., 32, 21, doi:10.1029/2005GL023954, 2005. 8019

Dellino, P., Dioguardi, F., Mele, D., D'Addabbo, M., Zimanowski, B., Büttner, R., Doronzo, D. M., Sonder, I., Sulpizio, R., Dürig, T., and La Volpe, L.: Volcanic jets, plumes, and collapsing fountains: evidence from large-scale experiments, with particular emphasis on the entrainment rate, B. Volcanol., 76, 1–18, doi:10.1007/s00445-014-0834-6, 2014. 8020

de' Michieli Vitturi, M., Neri, A., and Barsotti, S.: PLUME-MoM 1.0: A new integral model of volcanic plumes based on the method of moments, Geosci. Model Dev., 8, 2447–2463, doi:10.5194/gmd-8-2447-2015, 2015. 8012, 8013

Devenish, B.: Using simple plume models to refine the source mass flux of volcanic eruptions according to atmospheric conditions, J. Volcanol. Geoth. Res., 256, 118–127, doi:10.1016/j.jvolgeores.2013.02.015, 2013. 8012, 8021

Dosio, A., Vila-Guerau de Arelano, J., and Holstlag, A.: Relating Eulerian and Lagrangian statistics for the turbulent dispersion in the atmospheric convective boundary layer, J. Atmos. Sci., 62, 1175–1191, 2005. 8038

Durant, A. J., Rose, W. I., Sarna-Wojcicki, A. M., Carey, S., and Volentik, A.: Hydrometeor-enhanced tephra sedimentation: constraints from the 18 May 1980 eruption of Mount St. Helens, J. Geophys. Res.-Sol. Ea., 114, 204, doi:10.1029/2008JB005756, 2009. 8012, 8024



Ernst, G., Sparks, R. S. J., Carey, S., and Bursik, M.: Sedimentation from turbulent jets and plumes, J. Geophys. Res., 101, 5575–5589, doi:10.1029/95JB01900, 1996. 8012, 8015, 8019

Esposti Ongaro, T., Cavazzoni, C., Erbacci, G., Neri, A., and Salvetti, M.: A parallel multiphase flow code for the 3D simulation of explosive volcanic eruptions, Parallel Comput., 33, 541–560, doi:10.1016/j.parco.2007.04.003, 2007. 8011

Folch, A.: A review of tephra transport and dispersal models: evolution, current status, and future perspectives, J. Volcanol. Geoth. Res., 235–236, 96–115, 2012. 8011, 8032, 8034

Folch, A., Costa, A., and Macedonio, G.: FALL3D: a computational model for transport and deposition of volcanic ash, Comput. Geosci., 35, 1334–1342, doi:10.1016/j.cageo.2008.08.008, 2009. 8019

Folch, A., Costa, A., Durant, A., and Macedonio, G.: A model for wet aggregation of ash particles in volcanic plumes and clouds: 2. Model application, J. Geophys. Res., 115, B09202, doi:10.1029/2009JB007176, 2010. 8012, 8017, 8024, 8025, 8033

Frenklach, M.: Method of moments with interpolative closure, Chem. Eng. Sci., 57, 2229–2239, 2002. 8025

Ganser, G. H.: A rational approach to drag prediction of spherical and nonspherical particles, Powder Technol., 77, 143–152, doi:10.1016/0032-5910(93)80051-B, 1993. 8019

Gmachowski, L.: Calculation of the fractal dimension of aggregates, Colloid. Surfaces A, 211, 197–203, doi:10.1016/S0927-7757(02)00278-9, 2002. 8026

Gudmundsson, M., Thordarson, T., Höskuldsson, A., Larsen, G., Björnsson, H., Prata, F., Oddsson, B., Magnüsson, E., Högnadoóttir, T., Petersen, G., Hayward, C., Stevenson, J., and Jónsdóttir: Ash generation and distribution from the April-May 2010 eruption of Eyjafjallajökull, Iceland, Scientific Reports, 1–12, doi:10.1038/srep00572, 2012. 8034, 8035

Herzog, M. and Graf, H.-F.: Applying the three-dimensional model ATHAM to volcanic plumes: dynamic of large co-ignimbrite eruptions and associated injection heights for volcanic gases, Geophys. Res. Lett., 37, 19, doi:10.1029/2010GL044986, 2010. 8011

Hewett, T. A., Fay, J. A., and Hoult, D. P.: Laboratory experiments of smokestack plumes in a stable atmosphere, Atmos. Environ., 5, 767–789, doi:10.1016/0004-6981(71)90028-X, 1971. 8020

Hindmarsh, A.: Lsode and lsodi, two new initial value ordinary differential equations solvers, Acm-Signum Newsl., 4, 10–11, 1980. 8031

Jacobson, M. Z.: Fundamentals of Atmospheric Modelling, 2nd edn., Cambridge University Press, New York, 2005. 8027
Jullien, R. and Botet, R.: Aggregation and Fractal Aggregates, World Sci., Singapore, 1987. 8025
Kaminski, E., Tait, S., and Carazzo, G.: Turbulent entrainment in jets with arbitrary buoyancy, J. Fluid Mech., 526, 361–376, doi:10.1017/S0022112004003209, 2005. 8021, 8049
Krumbein, W. C.: Size frequency distributions of sediments, J. Sediment. Res., 4, 65–67, 1934. 8013
Mastin, L. G.: A user-friendly one-dimensional model for wet volcanic plumes, Geochem. Geophy. Geosy., 8, 3, doi:10.1029/2006GC001455, 2007. 8012
Mastin, L., Guffanti, M., Servranckx, R., Webley, P., Barsotti, S., Dean, K., Durant, A., Ewert, J., Neri, A., Rose, W., Schneider, D., Siebert, L., Stunder, B., Swanson, G., Tupper, A., Volentik, A., and Waythomas, C.: A multidisciplinary effort to assign realistic source parameters to models of volcanic ash-cloud transport and dispersion during eruptions, improved prediction and tracking of volcanic ash clouds, J. Volcanol. Geoth. Res., 186, 10–21, doi:10.1016/j.jvolgeores.2009.01.008, 2009. 8011
Morton, B. R., Taylor, G. I., and Turner, J. S.: Turbulent gravitational convection from maintained and instantaneous source, P. R. Soc. London, 234, 1–23, 1956. 8011, 8020
Murphy, D. M. and Koop, T.: Review of the vapour pressures of ice and supercooled water for atmospheric applications, Q. J. Roy. Meteor. Soc., 131, 1539–1565, doi:10.1256/qj.04.94, 2005. 8017
Netterville, D. D. J.: Plume rise, entrainment and dispersion in turbulent winds, Atmos. Environ.-A. Gen., 24, 1061–1081, 1990. 8015
Pruppacher, H. R. and Klett, J. D.: Microphysics of Clouds and Precipitation, 1st edn., Springer, ISBN: 978-0-7923-4211-3 (Print) Boston Kluwer Academic Publishers, 1996. 8027
Rose, W. and Durant, A.: El Chichón volcano, April 4, 1982: volcanic cloud history and fine ash fallout, Nat. Hazards, 51, 363–374, doi:10.1007/s11069-008-9283-x, 2009. 8032, 8033, 8058
Rouse, H., Yih, C. S., and Humphreys, H. W.: Gravitational convection from a boundary source, Tellus, 4, 201–210, 1952. 8049
Schneider, D. J., Rose, W. I., Coke, L. R., and Bluth, G. J. S.: Early evolution of a stratospheric volcanic eruption cloudas observed with TOMS and AVI-IRR, J. Geophys. Res., 104, 4037–4050, 1999. 8034





Sigurdsson, H., Carey, S., and Espindola, J.: The 1982 eruptions of El Chichón Volcano, Mexico: stratigraphy of pyroclastic deposits, J. Volcanol. Geoth. Res., 23, 11–37, doi:10.1016/0377-0273(84)90055-6, 1984. 8032
Sparks, R.: The dimensions and dynamics of volcanic eruption columns, B. Volcanol., 48, 3–15, doi:10.1007/BF01073509, 1986. 8011, 8023
Sparks, R. S. J., Bursik, M. I., Carey, S. N., Gilbert, J., Glaze, L. S., Sigurdsson, H., and Woods, A.: Volcanic Plumes, Wiley, Chichester, 574 p., 1997. 8010
Suzuki, Y. J. and Koyaguchi, T.: A three-dimensional numerical simulation of spreading umbrella clouds, J. Geophys. Res., 114, B03209, doi:10.1029/2007JB005369, 2009. 8011, 8020
Suzuki, Y. J. and Koyaguchi, T.: 3D numerical simulation of volcanic eruption clouds during the 2011 Shinmoe-dake eruptions, Earth Planets Space, 65, 581–589, doi:10.5047/eps.2013.03.009, 2013. 8011, 8021
Suzuki, Y. J. and Koyaguchi, T.: Effects of wind on entrainment efficiency in volcanic plumes, J. Geophys. Res., accepted, doi:10.1002/2015JB012208, 2015. 8021
Suzuki, Y. J., Koyaguchi, T., Ogawa, M., and Hachisu, I.: A numerical study of turbulent behaviour in eruption clouds using a three dimensional fluid dynamics model, J. Geophys. Res., 110, B08201, doi:10.1029/2004JB003460, 2005. 8011
Tate, P. M.: The rise and dilution of buoyant jets and their behaviour in an internal wave field, PhD thesis, University of New South Wales, available at: http://trove.nla.gov.au/version/19798635 (last access: 16 September 2015), 2002. 8022
Wilson, L.: Explosive volcanic eruptions, III. Plinian eruption columns, Geophys. J. Int., 45, 543–556, doi:10.1111/j.1365-246X.1976.tb06909.x, 1976. 8011
Wilson, L. and Huang, T. C.: The influence of shape on the atmospheric settling velocity of volcanic ash particles, Earth Planet. Sc. Lett., 44, 311–324, doi:10.1016/0012-821X(79)90179-1, 1979. 8019
Woodhouse, M. J., Hogg, A. J., Phillips, J. C., and Sparks, R. S. J.: Interaction between volcanic plumes and wind during the 2010 Eyjafjallajökull eruption, Iceland, J. Geophys. Res.-Sol. Ea., 118, 92–109, doi:10.1029/2012JB009592, 2013. 8012, 8015, 8017
Woods, A.: The fluid dynamics and thermodynamics of eruption columns, B. Volcanol., 50, 169–193, 1988. 8011
Woods, A. W.: Moist convection and the injection of volcanic ash into the atmosphere, J. Geophys. Res., 98, 17627, doi:10.1029/93JB00718, 1993. 8011, 8015, 8017, 8018, 8021

Woods, A. W. and Kienle, J.: The dynamics and thermodynamics of volcanic clouds: theory and observations from the April 15 and April 21, 1990 eruptions of Redoubt Volcano, Alaska, J. Volcanol. Geoth. Res., 62, 273–299, 1994. 8023

Xiong, C. and Friedlander, S. K.: Morphological properties of atmospheric aerosol aggregates, P. Natl. Acad. Sci. USA, 98, 11851–11856, doi:10.1073/pnas.211376098, 2001. 8025, 8026




**Table 1.** List of latin symbols. Quantities with a hat denote bulk (top-hat averaged) quantities. Throughout the text, the subindex o (e.g. $\hat{M}_o$, $\hat{u}_o$, etc.) indicates values of quantities at the vent ($s = 0$).

| Symbol | Definition | Units | Comments |
|---|---|---|---|
| $A_i^+ (A_i^-)$ | Aggregation source (sink) terms | $kg\,s^{-1}\,m^{-1}$ | Given by Eqs. (28) and (29) |
| $A_B$ | Collision frequency by Brownian motion | $m^3\,s^{-1}$ | Given by Eq. (41a) |
| $A_{DS}$ | Collision frequency by differential sedimentation | $m^{-1}s^{-1}$ | Given by Eq. (41c) |
| $A_S$ | Collision frequency by fluid shear | $s^{-1}$ | Given by Eq. (41b) |
| $A_{TI}$ | Collision frequency by turbulent inertia | $m^3\,s^{-1}$ | Given by Eq. (41d) |
| $\hat{c}$ | Specific heat capacity of the mixture | $J\,kg^{-1}\,K^{-1}$ | Given by Eq. (12) |
| $c_a$ | Specific heat capacity of air at constant pressure | $J\,kg^{-1}\,K^{-1}$ | Default value 1000 |
| $c_l$ | Specific heat capacity of liquid water | $J\,kg^{-1}\,K^{-1}$ | Default value 4200 |
| $c_p$ | Specific heat capacity of particles (pyroclasts) | $J\,kg^{-1}\,K^{-1}$ | Default value 1600 |
| $c_s$ | Specific heat capacity of solid water (ice) | $J\,kg^{-1}\,K^{-1}$ | Default value 2000 |
| $c_v$ | Specific heat capacity of water vapor | $J\,kg^{-1}\,K^{-1}$ | Default value 1900 |
| $C_d$ | Particle drag coefficient | – | Given by Eq. (15) |
| $\hat{C}_i$ | Mass concentration of particles of class *i* | $kg\,m^{-3}$ | Given by Eq. (43) |
| $D_f$ | Fractal exponent | – | Values between 2.8 and 3 (Costa et al., 2010) |
| $d_A$ | Diameter of the aggregates | m | One single aggregated class is assumed |
| $d_i$ | Diameter of particles of class *i* | m | Sphere equivalent diameter for irregular shapes |
| $e_l$ | Saturation pressure of water vapor over liquid | Pa | Given by Eq. (6) |
| $e_s$ | Saturation pressure of water vapor over solid (ice) | Pa | Given by Eq. (7) |
| $\hat{E}$ | Energy flow rate | $kg\,m^2\,s^{-3}$ | $\hat{E} = \hat{M}\left(\hat{c}\hat{T} + gz + \frac{1}{2}\hat{u}^2\right)$ |
| $\hat{f}$ | Correction factor for aggregation | – | See Appendix A. Values between 2–4. |
| $f$ | Particle re-entrainment parameter | – | Given by Eq. (13) |
| $f_i$ | Mass fraction of particle class *i* | – | $\sum f_i = 1$ |
| $g$ | Gravitational acceleration | $ms^{-2}$ | Value of 9.81 |
| $k_b$ | Boltzmann constant | $JK^{-1}$ | Value of $1.38 \times 10^{-23}$ |
| $L_c$ | Latent heat of water vapor condensation | $J\,kg^{-1}$ | Given by Eq. (10) |
| $L_d$ | Latent heat of water vapor deposition | $J\,kg^{-1}$ | Given by Eq. (11) |
| $\hat{M}$ | Total mass flow rate | $kg\,s^{-1}$ | $\hat{M} = \pi r^2 \hat{\rho}\hat{u} = \sum \hat{M}_i + \hat{M}_w + \hat{M}_a$ |
| $\hat{M}_a$ | Mass flow rate of dry air | $kg\,s^{-1}$ | |
| $\hat{M}_i$ | Mass flow rate of particles of class *i* | $kg\,s^{-1}$ | $\hat{M}_i = \hat{M}\hat{x}_p f_i$ |
| $\hat{M}_w$ | Mass flow rate of volatiles (water in any phase) | $kg\,s^{-1}$ | $\hat{M}_w = \hat{M}\hat{x}_w$ |
| $N_i$ | Number of particles of diameter $d_i$ in an aggregate | – | Given by Eq. (31) |
| $\dot{n}_i$ | Number of aggregating particles per unit volume and time | $m^{-3}s^{-1}$ | Given by Eq. (30) |
| $\dot{n}_{tot}$ | Total particle decay per unit volume and time | $m^{-3}s^{-1}$ | Given by Eq. (34) |
| $n_{tot}$ | Number of particles per unit volume available for aggregation | $m^{-3}$ | Given by Eq. (42) |
| $\hat{P}$ | Axial (stream-wise) momentum flow rate | $kg\,m\,s^{-2}$ | $\hat{P} = \hat{M}\hat{u}$ |
| $P$ | Pressure | Pa | |
| $P_v$ | Partial pressure of water vapor | Pa | Given by Eq. (5) |
| $r$ | Cross-section plume radius | m | Axial symmetry is assumed |

**Table 1.** Continued.

| Symbol | Definition | Units | Comments |
|---|---|---|---|
| $s$ | Distance along the plume axis | m | Equations integrated from $s = 0$ to the NBL |
| $\hat{T}$ | Mixture temperature | K | Thermal equilibrium is assumed |
| $T_a$ | Ambient air temperature | K | Assumed to vary only with $z$ |
| $T_f$ | Freezing temperature | K | Value of 255 ($-18\,^{\circ}$C) assumed |
| $\hat{u}$ | Mixture velocity along the plume axis | $m\,s^{-1}$ | Mechanical equilibrium is assumed |
| $u_a$ | Horizontal wind (air) velocity | $m\,s^{-1}$ | Assumed to vary only with $z$ |
| $u_e$ | Air entrainment velocity (by turbulent eddies) | $m\,s^{-1}$ | Given by Eq. (17) |
| $u_{si}$ | Terminal settling velocity of particle class $i$ | $m\,s^{-1}$ | Given by Eq. (14) |
| $w_a$ | Mass fraction of water in the entrained ambient air | – | Specific humidity (kg/kg) |
| $x$ | Horizontal coordinate | m | |
| $\hat{x}_l$ | Mass fraction of liquid water | – | |
| $\hat{x}_s$ | Mass fraction of solid water (ice) | – | |
| $\hat{x}_v$ | Mass fraction of water vapor | – | |
| $\hat{x}_p$ | Mass fraction of particles (pyroclasts) | – | Given by Eq. (4) |
| $\hat{x}_w$ | Mass fraction of volatiles (water) | – | $\hat{x}_w = \hat{x}_v + \hat{x}_l + \hat{x}_s$ |
| $y$ | Horizontal coordinate | m | |
| $z$ | Vertical coordinate | m | Typically given a.s.l. or a.v.l. |
| $z_s$ | Dimensionless height | – | $z_s = z/2r_o$ |





**Table 2.** List of greek symbols. Quantities with a hat denote bulk (top-hat averaged) quantities.

| Symbol | Definition | Units | Comments |
|---|---|---|---|
| $\alpha_m$ | Class-averaged particle sticking efficiency | – | Given by Eq. (44) |
| $\alpha_{ij}$ | Sticking efficiency between particles of class $i$ and $j$ | – | Given by Eq. (45) |
| $\alpha_s$ | stream-wise (shear) air entrainment coefficient | – | Given by Eq. (19) |
| $\alpha_v$ | cross-flow (vortex) air entrainment coefficient | – | Given by Eq. (21) |
| $\epsilon$ | Dissipation rate of turbulent kinetic energy | $m^2 s^{-3}$ | Given by Eq. (37) |
| $\Gamma_s$ | Fluid shear | $s^{-1}$ | Given by Eq. (39) |
| $\phi$ | Volume fraction of particles | – | |
| $\hat{\mu}$ | Mixture dynamic viscosity | Pa s | Assumed equal to that of air at bulk temperature |
| $\mu_l$ | Liquid water dynamic viscosity | Pa s | |
| $\hat{\nu}$ | Mixture kinematic viscosity | $m^2 s^{-1}$ | $\hat{\nu} = \hat{\mu}/\hat{\rho}$ |
| $\hat{\rho}$ | Mixture density | $kg\,m^{-3}$ | Given by Eq. (3) |
| $\rho_a$ | Ambient air density | $kg\,m^{-3}$ | Assumed to vary only with $z$ |
| $\rho_l$ | Liquid water density | $kg\,m^{-3}$ | Value of 1000 |
| $\rho_g$ | Gas phase (dry air plus water vapor) density | $kg\,m^{-3}$ | |
| $\rho_p$ | Class-averaged particle (pyroclasts) density | $kg\,m^{-3}$ | $\rho_p = \sum f_i \rho_{pi}$ |
| $\rho_{pi}$ | Density of particles of class $i$ | $kg\,m^{-3}$ | |
| $\rho_s$ | Ice density | $kg\,m^{-3}$ | Value of 920 |
| $\phi$ | Solid (particles) volume fraction | – | $\phi = \sum \hat{C}_i/\rho_{pi}$ |
| $\Phi$ | Dimensionless number related to size | – | Given by Eq. (1) |
| $\Phi_a$ | Horizontal wind direction (azimuth) | rad | |
| $\Psi$ | Particle sphericity | – | $\Psi = 1$ for spheres |
| $\theta$ | Plume bent over angle with respect to the horizontal | rad | |
| $\xi$ | Diameter to volume fractal relationship | – | |
| $\chi$ | Constant giving the probability of fallout | – | Value of $\approx 0.23$(Bursik, 2001) |

**Table 3.** Constants defining the entrainment functions for jets and plumes following the formulation introduced by Kaminski et al. (2005) (see Eq. 20a to 20c) obtained after fitting experimental data reported in Carazzo et al. (2006). For Kaminski-R we considered all data including that of Rouse et al. (1952), whereas for Kaminski-C, as suggested by Carazzo et al. (2006), data from Rouse et al. (1952) was excluded.

| | Kaminski-R | | Kaminski-C | |
|---|---|---|---|---|
| | jets | plumes | jets | plumes |
| $c_0$ | 1.92 | 1.61717 | 1.92 | 1.55 |
| $c_1$ | 3737.26 | 478.374 | 3737.26 | 329.0 |
| $c_2$ | 4825.98 | 738.348 | 4825.98 | 504.5 |
| $c_3 = 2(c_2 - c_1)$ | 2177.44 | 519.948 | 1883.81 | 351.0 |
| $c_4$ | 0.00235 | −0.00145 | 0.00235 | −0.00145 |





**Table 4.** Input values for the El Chichón Phase-B simulation. Values for specific heats of water vapour, liquid water, ice, pyroclasts and air at constant pressure are assigned to defaults of 1900, 4200, 2000, 1600, and 1000 $\mathrm{J\,kg^{-1}\,K^{-1}}$.

| Parameter | Symbol | Units | Value |
|---|---|---|---|
| Phase start | | h | 1:35 UTC |
| Phase end | | h | 6:00 UTC |
| Exit velocity | $\hat{u}_o$ | $\mathrm{m\,s^{-1}}$ | 350 |
| Exit temperature | $\hat{T}_o$ | K | 1123 |
| water ~~Magmatic~~ mass fraction | $\hat{w}_o$ | – | 4 % |
| Diameter aggregates | $d_A$ | µm | 250 |
| Density aggregates | $\hat{\rho}_A$ | $\mathrm{kg\,m^{-3}}$ | 200 |
| Probability of particle fallout | $\chi$ | – | 0.23 |
| Shear entrainment coefficient | $\alpha_s$ | – | Eq. (19) |
| Vortex entrainment coefficient | $\alpha_v$ | – | Eq. (21) |



Discussion Paper | Discussion Paper | Discussion Paper | Discussion Paper |

**Table 5.** FPLUME input values for the 6 May Eyjafjallajökull simulation. Values for specific heats of water vapour, liquid water, ice, pyroclasts and air at constant pressure are assigned to defaults of 1900, 4200, 2000, 1600, and 1000 $\mathrm{J\,kg^{-1}\,K^{-1}}$.

| Parameter | Symbol | Units | Value |
|---|---|---|---|
| Phase start | | h | 06:00 UTC |
| Phase end | | h | 12:00 UTC |
| Exit velocity | $\hat{u}_o$ | $\mathrm{m\,s^{-1}}$ | 150 |
| Exit temperature | $\hat{T}_o$ | K | 1200 |
| Water ~~Magmatic~~ mass fraction | $\hat{w}_o$ | – | 3 % |
| Diameter aggregates | $d_A$ | µm | 500 |
| Density aggregates | $\hat{\rho}_A$ | $\mathrm{kg\,m^{-3}}$ | 200 |
| Probability of particle fallout | $\chi$ | – | 0.23 |
| Shear entrainment coefficient | $\alpha_s$ | – | Eq. (19) |
| Vortex entrainment coefficient | $\alpha_v$ | – | Eq. (21) |



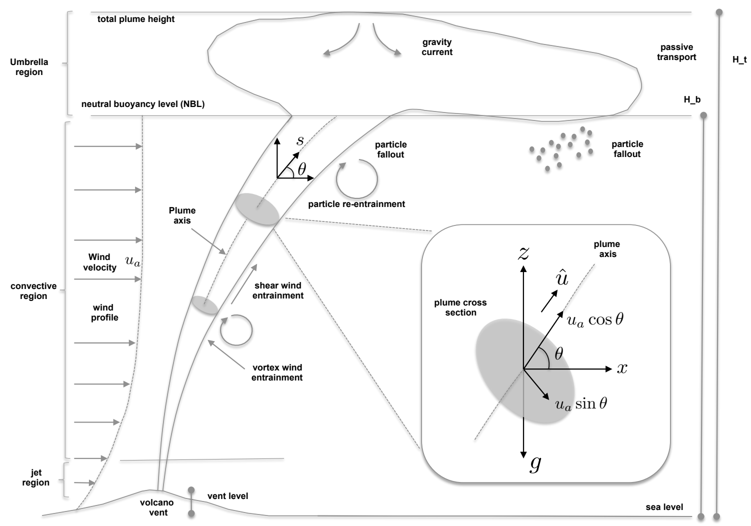


**Figure 1.** Sketch of an axisymmetric volcanic plume raising in a wind profile. Three different regions (jet thrust, convective thrust and umbrella) are indicated, with the convective region reaching a height $H_b$ (that of the neutral buoyancy level), and the umbrella region raising up to $H_t$ above the sea level (a.s.l.). The inset plot details a plume cross-section perpendicular to the plume axis, inclined of an angle $\theta$ with respect to the horizontal.




Discussion Paper | Discussion Paper | Discussion Paper | Discussion Paper |

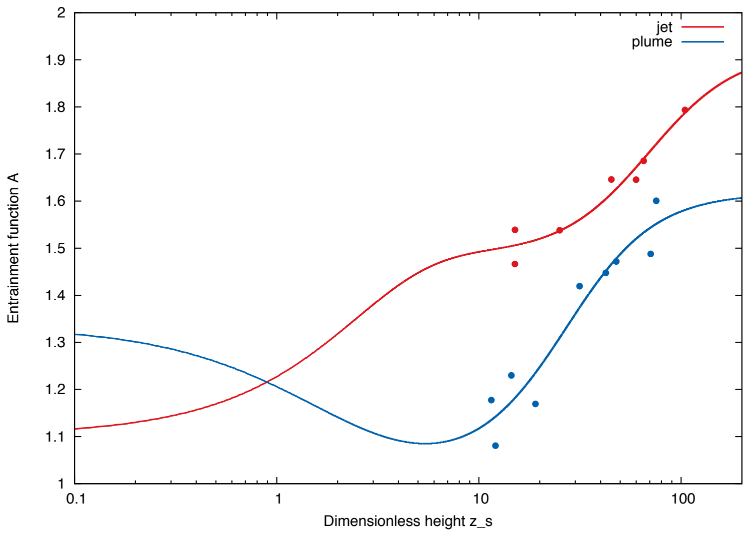


**Figure 2.** Entrainment functions $A(z_s)$ for jets and plumes depending on the dimensionless height $z_s = z/2r_o$. Functions have been obtained by fitting experimental data (points) from Carazzo et al. (2006) (for $z_s > 10$) and multiplying by a correction function (20c) to extend the functions to $z_s < 10$ verifying function continuity and convergence to values of $A = 1.11$ for jets and $A = 1.31$ for plumes when $z_s \rightarrow 0$.





*I suggest plotting in non-dimensional scale Zs*

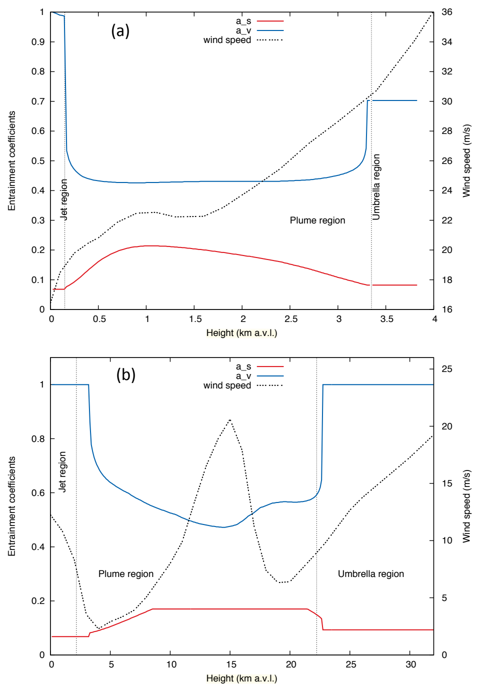


**Figure 3.** Entrainment coefficients $\alpha_s$ (red) and $\alpha_v$ (blue) vs. height for weak **(a)** and strong **(b)** plumes under a wind profile. The vertical dashed lines indicate the transition between the different eruptive column regions. Weak plume simulation with: $\hat{M}_o = 1.5 \times 10^6\,\mathrm{kg\,s^{-1}}$, $\hat{u}_o = 135\,\mathrm{m\,s^{-1}}$, $\hat{T}_o = 1273\,\mathrm{K}$, $\hat{x}_{wo} = 0.03$. Strong plume simulation with: $\hat{M}_o = 1.5 \times 10^9\,\mathrm{kg\,s^{-1}}$, $\hat{u}_o = 300\,\mathrm{m\,s^{-1}}$, $\hat{T}_o = 1153\,\mathrm{K}$, $\hat{x}_{wo} = 0.05$.

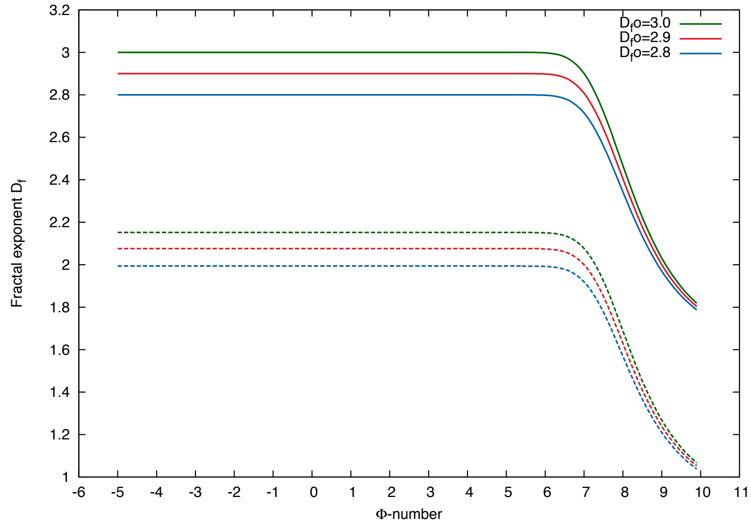


**Figure 4.** Dependency of fractal exponent $D_f$ (continuous lines) and fractal pre-factor $k_f$ (dashed lines) on particle size expressed in Φ units according to equations (32) and (33) for different values of $D_{fo}$. Note the progressive decay in $D_f$ starting at $\Phi = 7$ ($d \approx 10\,\mu$m) and leading to values of $D_f = 1.6$ for $\Phi = 9$ ($d \approx 2\,\mu$m).



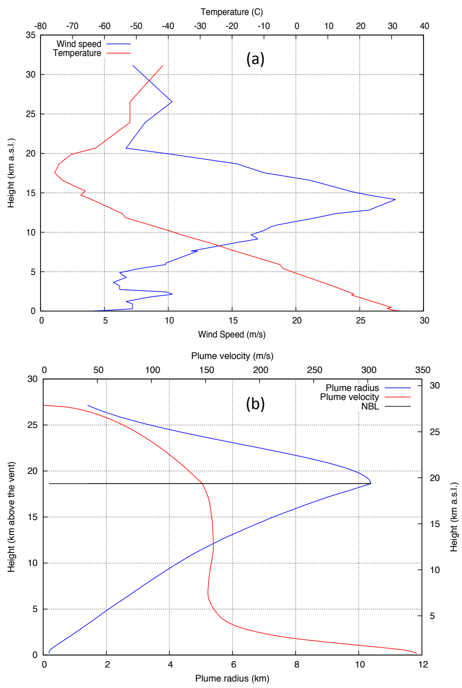


**Figure 5. (a)**: wind and temperature atmospheric profiles during 4 April 1982 at 00:00 UTC from sounding. **(b)**: FPLUME bulk velocity $\hat{u}$ and radius $r$ with height $z$. The black solid line indicates the height of the NBL determined by the model.

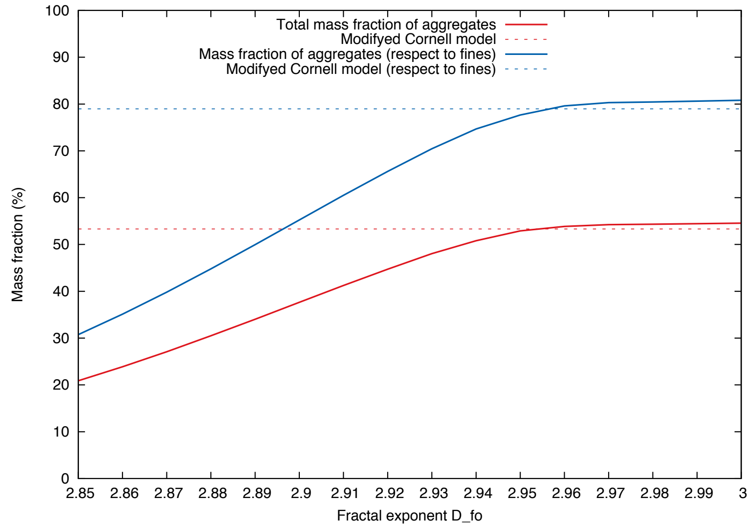


**Figure 6.** El Chichón 1982 phase-B simulation. Total mass fraction of aggregates (red line) and total mass fraction of aggregates with respect to fines (blue line) depending on the fractal exponent $D_{\mathrm{fo}}$. The (constant) values predicted by the modified Cornell model are shown by dashed lines.



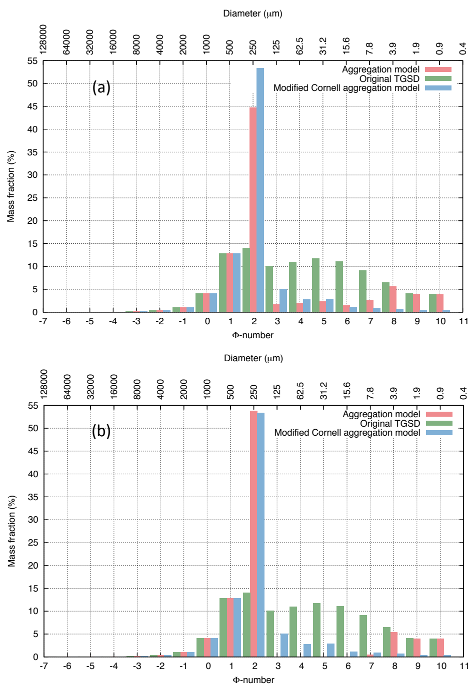


**Figure 7.** Results of the aggregation model in FPLUME for El Chichón 1982 phase-B simulation. Green bars show the original TGSD from Rose and Durant (2009) discretized in 17 Φ-classes. Blue bars show the results of the modified Cornell model. Finally, read bars give the results of our wet aggregation model considering a fractal exponent of $D_{\mathrm{fo}} = 2.96$ **(a)** and $D_{\mathrm{fo}} = 2.92$ **(b)**.

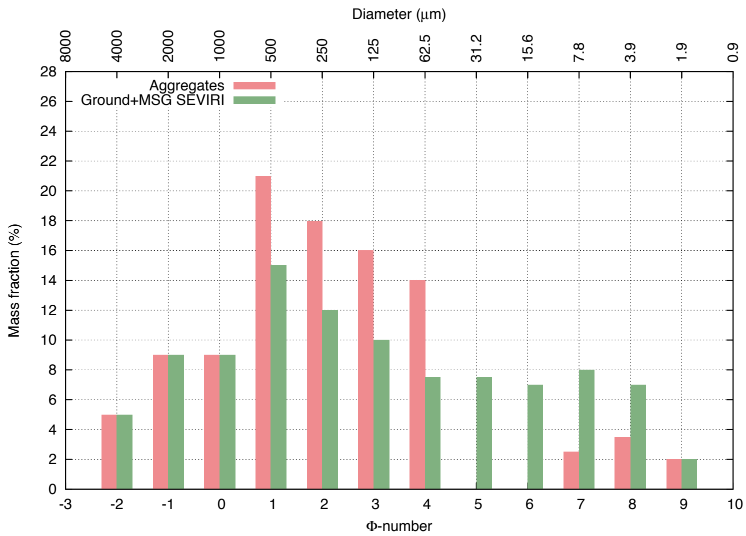


**Figure 8.** Original grain size distribution from ground data and MSG-SEVIRI retrievals (green) and distribution modified by aggregation (red). Results are for 6 May 30 min averaged. Figure reproduced from Bonadonna et al. (2011) (Fig. 17d).





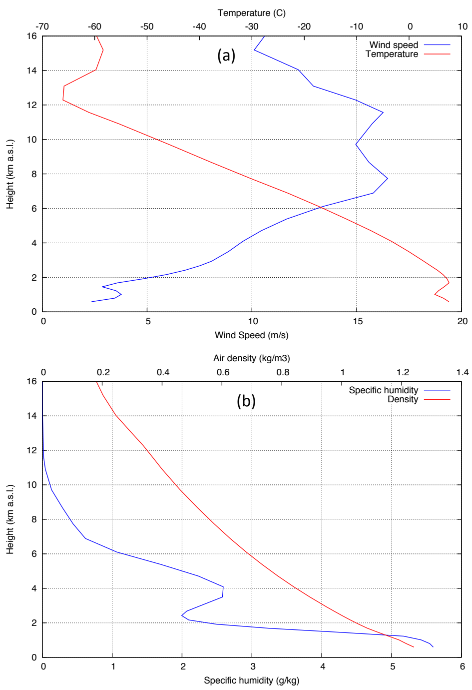


**Figure 9.** Atmospheric profiles extracted form ERA-Interim re-analysis dataset at Eyjafjallajökull vent location for 6 May 2010 at 12:00 UTC. **(a)**: wind and temperature profiles. **(b)**: specific humidity and air density profiles.

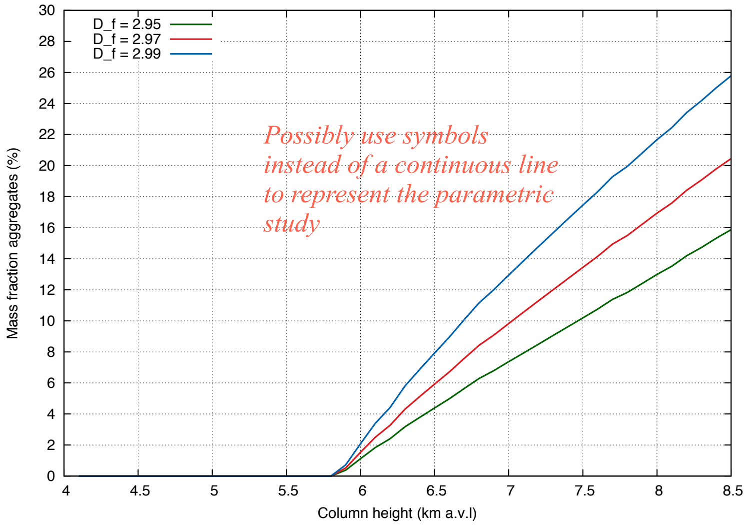


**Figure 10.** FPLUME aggregation model results for Eyjafjallajökull 6 May phase. Total mass fraction of aggregates (in %) vs. column height (in km a.v.l.) for different values of the fractal exponent $D_{fo}$. The model predicts a 10 % in mass of wet aggregates for column heights between 6.7 and 7.5 km (a.v.l.).





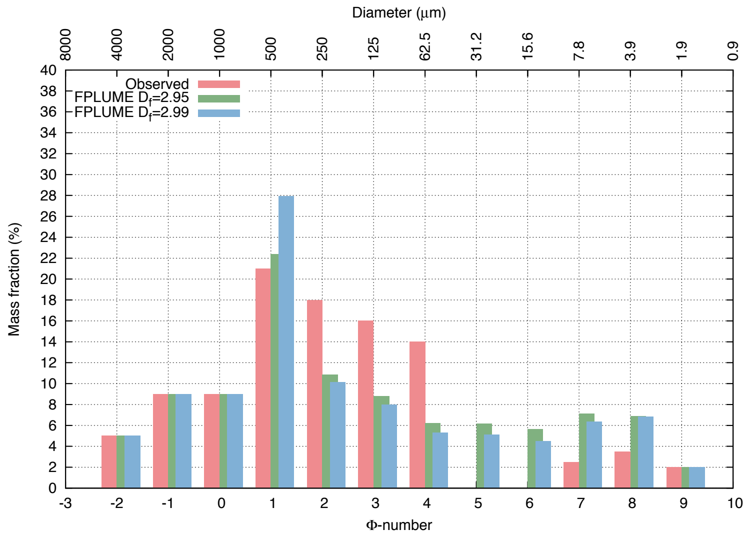


**Figure 11.** Grain size distribution predicted by the wet aggregation model for Eyjafjallajökull 6 May phase for a column height of 7 km (a.v.l.) for two different values of the fractal exponent $D_{fo}$ of 2.95 and 2.99. Observed data from Bonadonna et al. (2011).